Dynamics of meandering spiral waves with weak lattice perturbations

Petko M. Kitanov
Department of Mathematics and Statistics
University of Ottawa
Ottawa, ON K1N 6N5
CANADA

Victor G. LeBlanc
Department of Mathematics and Statistics
University of Ottawa
Ottawa, ON K1N 6N5
CANADA

December 13, 2016

Abstract

Re-entrant spiral waves are observed in many different situations in nature, perhaps most importantly in excitable electrophysiological tissue where they are believed to be responsible for pathological conditions such as cardiac arrhythmias, epileptic seizures and hallucinations. Mathematically, spiral waves occur as solutions to systems of reaction-diffusion partial differential equations (RDPDEs) which are frequently used as models for electrophysiological phenomena. Because of the invariance of these RDPDEs with respect to the Euclidean group $\mathbf{SE}(2)$ of planar translations and rotations, much progress has been made in understanding the dynamics and bifurcations of spiral waves using the theory of group-equivariant dynamical systems. In reality however, Euclidean symmetry is at best an approximation. Inhomogeneities and anisotropy in the medium of propagation of the waves break the Euclidean symmetry, and can lead to such phenomena as anchoring and drifting. In this paper, we study the effects on quasi-periodic meandering spiral waves of a small perturbation which breaks the continuous $\mathbf{SE}(2)$ symmetry, but preserves the symmetry of a regular square lattice.

1 Introduction

Spiral waves have been studied now extensively for a few decades since the pioneering work of Winfree [42, 43]. One of the most important reasons why they have been given so much attention is the mounting evidence that in electrophysiological tissue (such as the myocardium, the visual cortex or the brain), spiral waves are typically symptomatic of pathological conditions such as fibrillation, hallucinations, and epileptic seizures [13, 21, 22, 28, 32, 41].

A large class of mathematical models in which spiral waves occur as solutions are reaction-diffusion partial differential equations (RDPDEs) on planar domains,

$$\frac{\partial U}{\partial t}(x,y,t) = D \cdot \nabla^2 U(x,y,t) + f(U(x,y,t),\lambda), \tag{1.1}$$

where $U : \mathbb{R}^2 \times \mathbb{R}^+ \longrightarrow \mathbb{R}^N$ may represent, for example, electric potentials of different ions through cellular membranes, or concentrations of chemicals. The $N \times N$ constant matrix D determines diffusion coefficients, and $\nabla^2 = \frac{\partial^2}{\partial x^2} + \frac{\partial^2}{\partial y^2}$ is the Laplacian. The smooth function $f : \mathbb{R}^N \times \mathbb{R}^m \longrightarrow \mathbb{R}^N$ describes the local reaction kinetics of the model, and $\lambda \in \mathbb{R}^m$ are model parameters.

When (1.1) is posed on the whole plane, this equation admits an important symmetry property:*: whenever $U(x,y,t)$ is a solution of (1.1), then so is

$$S(x,y,t) = U(x\cos\,\phi - y\sin\,\phi + p_1, x\sin\,\phi + y\cos\,\phi + p_2, t)$$

for any angle ϕ in the circle group $\mathbf{S}^1$, and any $(p_1,p_2) \in \mathbb{R}^2$. In the jargon of dynamical systems theory, we say that the right-hand side of (1.1) is $\mathbf{SE}(2)$-*equivariant*, where $\mathbf{SE}(2)$ designates the group of all planar translations and rotations.

Barkley [6, 7, 8, 9] was the first to recognize the importance of $\mathbf{SE}(2)$ symmetry in describing the dynamics and bifurcations of spiral waves which were observed in numerical simulations of (1.1) and in physical experiments [27]. Essentially, Barkley argued that the continuous symmetries of $\mathbf{SE}(2)$ should lead to low-dimensional (finite) ODE models to describe the basic modes of propagation of spiral waves: uniform spatial rotation of the spiral wave around a fixed point in space, or two-frequency epicyclic meandering spiral waves, where the tip of the spiral wave rotates around a point which itself precesses (see, for example, Figures 2 and 4 below). Later, Sandstede, Scheel and Wulff [35, 36] proved mathematically how Barkley's finite-dimensional models are, in fact, center manifold reductions of (1.1) in the context of infinite-dimensional $\mathbf{SE}(2)$-equivariant dynamical systems. See also [15, 16].

*In fact, (1.1) also admits reflectional symmetries, but these will not be relevant for the purposes of this paper.

In this context, rigidly rotating spiral waves are examples of *relative equilibria*, and two-frequency epicyclic meandering waves are examples of *relative periodic solutions* (see [35, 36] for the precise mathematical definitions of these concepts).

In any real physical situation, it is clear that $\mathbf{SE}(2)$ symmetry is, at most, an approximation. Boundaries, nonplanar geometry, inhomogeneities, and anisotropy (which are all important in the electrophysiological contexts alluded to earlier) break translational and/or rotational symmetries. Moreover, there are several experimental studies illustrating how broken translational and/or rotational symmetries may lead to dynamic states for spiral waves which are inconsistent with Euclidean symmetry: anchoring of spiral waves around regions of inhomogeneities [13, 29], drifting along boundaries [46, 47], and phase-locking and/or drifting of two-frequency meandering waves in the bidomain model of cardiac electrophysiology [33, 34]. These experimental observations led to a program of research [10, 11, 12, 24, 25, 26] which sought to use the theoretical apparatus of the center-manifold theorems of [35, 36] to characterize generic effects of *forced symmetry-breaking* on relative equilibria and relative periodic solutions. As a basic paradigm to illustrate forced symmetry-breaking from $\mathbf{SE}(2)$, consider the following perturbation of (1.1):

$$\frac{\partial U}{\partial t}(x,y,t) = D \cdot \nabla^2 U(x,y,t) + f(U(x,y,t),\lambda) + \varepsilon g(U(x,y,t),x,y,\varepsilon), \tag{1.2}$$

where ε is a small parameter and g is some bounded function which depends nontrivially and explicitly on the spatial coordinates x and y. Whereas (1.2) admits full $\mathbf{SE}(2)$ symmetry when $\varepsilon = 0$, it typically only admits a subgroup $\Sigma \subset \mathbf{SE}(2)$ when $\varepsilon \neq 0$, however small ε may be. Depending on the physical situation that one wants to describe, the subgroup Σ is prescribed in advance. Using this approach, it was shown in [10, 24, 26] that spiral anchoring, boundary drifting, and phase-locking and/or drifting of meandering waves in anisotropic media are generic consequences of forced symmetry-breaking from $\mathbf{SE}(2)$ to Σ, for appropriate choices of Σ. In some sense, we can view the dynamical system generated by (1.2) with $\varepsilon \neq 0$ as being close to an $\mathbf{SE}(2)$-equivariant dynamical system, so we expect solutions of (1.2) to retain some of the features of the $\mathbf{SE}(2)$ symmetry (at least on a transient level), as well as features of a Σ-equivariant dynamical system.

1.1 Lattice symmetry-breaking

In a recent paper [12], we studied the case where Σ in (1.2) is the group of rotational and translational symmetries of a regular square lattice. Specifically, we characterized the effects of this symmetry-breaking on relative equilibria (i.e. uniformly rigidly rotating spiral waves, or linearly translating waves with retracting tip). In summary, we found that a generic lattice symmetry-breaking perturbation had the following possible effects on relative equilibria:

- Creation of so-called *anchored* rotating waves (i.e., rotating waves with a preferred center of rotation in space). The point of anchoring is not necessarily a point of the lattice, but if it is, then the meander path has a 90 degree spatiotemporal symmetry (advancing in phase the solution through one quarter of the period has the same effect as rotating the entire spiral tip path by 90 degrees about the lattice point of anchoring).

- Creation of two-frequency meandering waves, where one of the frequencies is small (of the order of the size of the perturbation). Again, these are anchored in space. If the point of anchoring coincides with a lattice point, then the overall meander path has the rotational symmetries of a square.

- Stabilization of the transition from rotating wave (with large radius of rotation) to a linearly translating wave (i.e. the retracting tip phenomenon; see [5]).

The motivation for studying lattice symmetry-breaking is twofold. First, whenever an RDPDE model such as (1.1) is used to describe electrophysiological waves, it is understood that this continuum model is obtained after some averaging and homogenization over the cellular structure of the tissue. However, if the size of the spiral wave (e.g., spiral step size) is comparable to the size of the cellular structure, then inhomogeneities generated by gap junctions between cells may have an influence on the dynamics of the spiral wave. See, for example, Figure 1 (taken from [3]) which illustrates the spatial distribution of cones in a cross section of the human retina.

As a first approximation, one may assume that the cells are arranged in a square grid, although one could argue that in certain regions of Figure 1, perhaps a hexagonal grid is closer to reality. In any event, our goal is to characterize the generic first order effects of a lattice structure on spiral dynamics, so the specific geometry of the lattice (i.e., square versus hexagonal) is secondary in light of this. We choose a square lattice to simplify the presentation, and for the second motivation described below.

A second motivation to study square lattice symmetry-breaking from $\mathbf{SE}(2)$ is to try to characterize effects of coarse spatial grids on the resolution of spiral wave dynamics in numerical simulations of (1.1). Although the RDPDE (1.1) enjoys full $\mathbf{SE}(2)$ symmetry, numerical integration schemes which involve finite difference spatial discretization possess only the symmetries of the lattice. So it is not unreasonable to expect that numerical integrations of (1.1) may reflect features which are characteristic of this grid symmetry while still being "close" to being fully $\mathbf{SE}(2)$ symmetric [11]. This is especially true if the grid is coarse in relation to the size of the spiral. As an illustration of this point, in Figure 2 below, we show the path of the tip of a meandering spiral wave for four different numerical

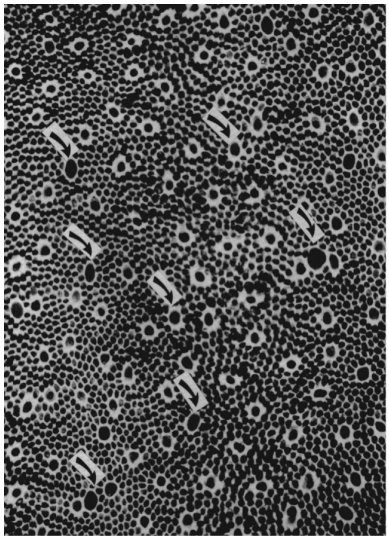

Figure 1: Figure 2 of [3] (with permission) illustrating the spatial arrangement of cones in a cross section of the human retina.

integrations of the FitzHugh-Nagumo system

$$\begin{aligned} \frac{\partial u}{\partial t} &= \nabla^2 u + \frac{1}{\tau}\left(u - \frac{1}{3}u^3 - v\right) \\ \frac{\partial v}{\partial t} &= \tau(u + \beta - \gamma v) \end{aligned} \tag{1.3}$$

on the domain $[-10\pi, 10\pi]^2$ using a finite difference scheme (explicit in time) with varying grid sizes and Neumann boundary conditions. In particular, there is phase-locking of a four-petal closed meandering path for a coarse grid, and this is inconsistent with Euclidean symmetry [9]. See also [1, 2, 38, 45] for further motivation as to the importance of understanding spiral wave dynamics in lattice structures.

As mentioned above, our emphasis in [12] was on characterizing the effects of lattice symmetry-breaking on relative equilibria. The goal of the present paper is to study the effects of this type of perturbation on relative periodic solutions (otherwise known as modulated rotating waves or modulated traveling waves [6, 7, 9]).

1.2 Numerical simulations

At several places in this paper, we will present results of numerical simulations to illustrate some of the features which are predicted from our analysis. These simulations are numerical

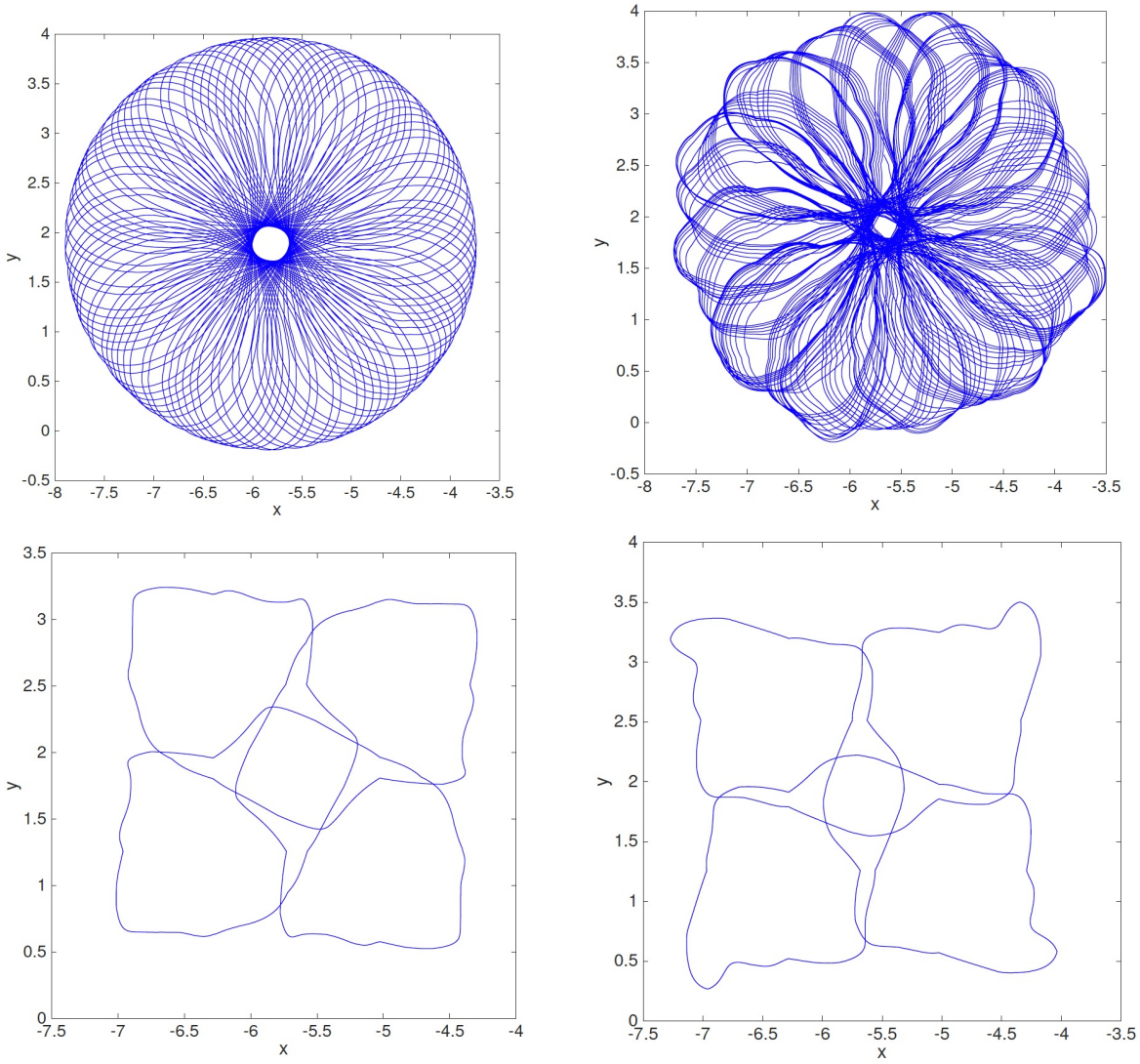

Figure 2: Path of the spiral tip for numerical integrations of (1.3) on the domain $[-10\pi, 10\pi]^2$ using a finite difference scheme (explicit in time) with varying grid sizes: 200×200 (top left), 100×100 (top right), 50×50 (bottom two figures). The same initial condition is used in all cases, and transients have been removed. The kinetic parameters are $\beta = 0.755$, $\gamma = 0.5$ (for all four figures), and $\tau = 0.2$ (both top figures and bottom left figure), or $\tau = 0.25$ (bottom right). The bottom figures illustrate a phase-locked four-petal closed meandering path with four-fold rotational symmetry, a result we will see in section 6 that is consistent with lattice symmetry-breaking.

integrations of the perturbed FitzHugh-Nagumo system

$$\begin{aligned} \frac{\partial u}{\partial t} &= \nabla^2 u + \frac{1}{\tau}\left(u - \frac{1}{3}u^3 - v\right) + \varepsilon\, g_1(x,y) \\ \frac{\partial v}{\partial t} &= \tau(u + \beta - \gamma v + \varepsilon\, g_2(x,y)) \end{aligned} \tag{1.4}$$

where $\nabla^2 = \frac{\partial^2}{\partial x^2} + \frac{\partial^2}{\partial y^2}$, τ, β, and γ are model parameters (which will be varied across the different simulations), the functions g_1 and g_2 are the lattice symmetry-breaking terms, and $\varepsilon \geq 0$ is a small parameter. When $\varepsilon = 0$, (1.4) reduces to (1.3), and is symmetric under the planar group of rotations and translations, $\mathbf{SE}(2)$. We will consider functions $g_{1,2}$ of the form

$$g_i = A_i + B_i(\cos(x/2) + \cos(y/2)) + C_i(\cos((3x-2y)/2) + \cos((2x+3y)/2)), \quad i = 1, 2, \tag{1.5}$$

where the coefficients A_i, B_i, and C_i will vary from simulation to simulation. Therefore, when $\varepsilon \neq 0$, the $\mathbf{SE}(2)$ symmetry of (1.4) is broken, but the rotational and translational symmetries of a square lattice are preserved. Simulations with more harmonic components and/or with sine components were also performed, but did not lead to any dynamics significantly different from those obtained using (1.5).

Definition 1.1 *For the perturbation functions g_i in (1.5), system (1.4) is invariant under transformations which are combinations of translations along the x or the y directions by integer multiples of 4π, and rotations around the origin by $\pi/2$. We will therefore refer to the points*

$$\{\, (4\pi n_1, 4\pi n_2) \mid n_1, n_2 \in \mathbb{Z} \,\}$$

as lattice points *in this paper. System (1.4) is also invariant under rotation by $\pi/2$ around the point $(2\pi, 2\pi)$. Hence, we will refer to the points*

$$\{\, (2\pi + 4\pi n_1, 2\pi + 4\pi n_2) \mid n_1, n_2 \in \mathbb{Z} \,\}$$

as dual lattice points *in this paper.*

Throughout this paper, in the several figures where we present results of numerical simulations of (1.4), we superimpose on the figure red squares and black crosses to guide the eye as to the position of the lattice points and the dual lattice points respectively (see Figure 6 for example).

For the numerical simulations which will be illustrated in this paper, the PDE (1.4) is integrated numerically on the rectangle $[-10\pi\,,\, 10\pi]^2$ using a finite-difference scheme ($200 \times$

200 spatial grid) and explicit time-stepping. Neumann boundary conditions are applied, and initial conditions are chosen so that the spiral tip is away from the edges, so that boundary effects (if any) should be negligible.

Fully symmetric case.

In Figure 3, we give a plot of the u and v components of a typical numerical integration of (1.4) when $\varepsilon = 0$, at a fixed instant in time, illustrating the spiral shape of the profile. To illustrate the meandering dynamics of spiral waves, we will track the position in space

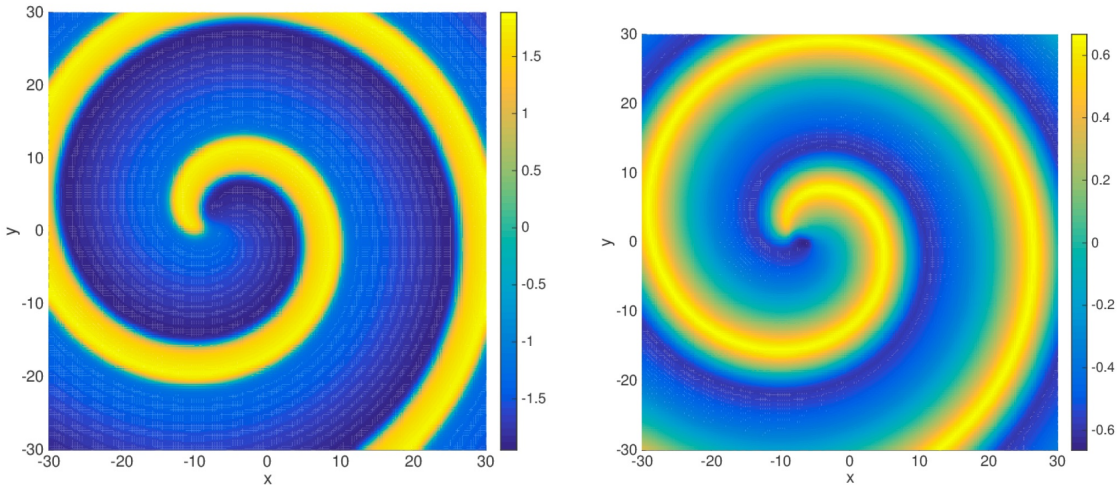

Figure 3: Plots of the u (left) and v (right) components at a fixed instant in time for a numerical integration of (1.4) with $\varepsilon = 0$ (homogeneous case), $\tau = 0.1858$, $\beta = 0.755$, $\gamma = 0.5$

of the "spiral tip," which we arbitrarily define in this paper as being the intersection of the $u = 0$ and $v = 0$ contours. Note that other definitions of the "tip" are possible, and it is well known [6, 7, 9, 33, 34] that the dynamics are qualitatively similar for different choices of definitions. In Figure 4, we give the position of the spiral tip for the integration of the homogeneous case described above and illustrated in Figure 3. We note that the meander path in Figure 4 resembles a flower with petals [15] pointing outward. Meander paths with inward pointing petals also occur in (1.4). Furthermore, in parameter space, there is a codimension-one surface across which meandering paths with outward petals change continuously into meandering paths with inward petals via *modulated traveling waves*, which

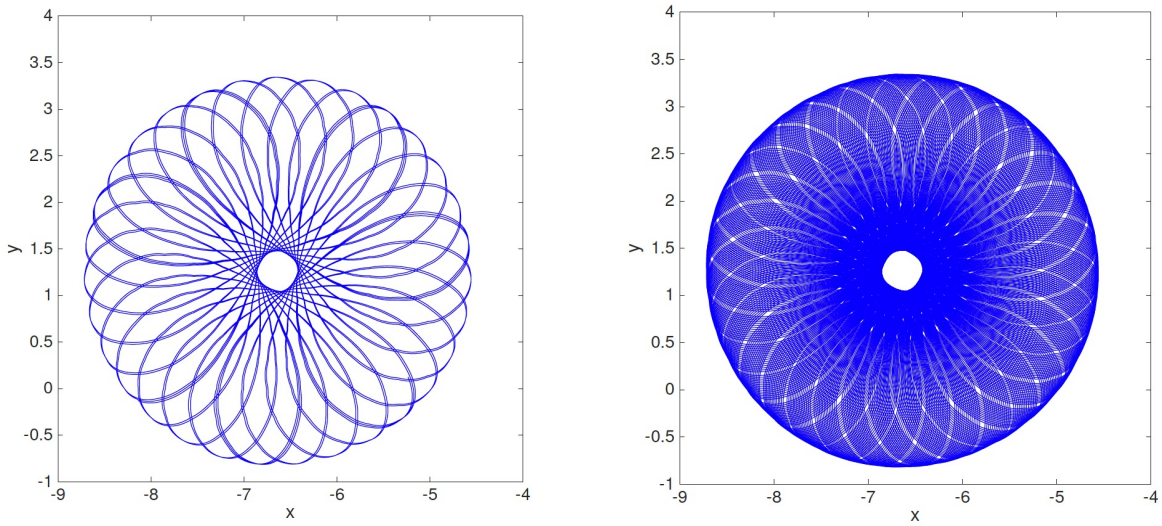

Figure 4: Plot in space of the position of the spiral tip for the integration described in Figure 3. The left figure is for a short integration time, and the right figure is for a longer integration time. This is typical of a two-frequency motion, where the frequencies are incommensurate.

are states where the spiral motion is characterized as a composition of a rotation and a linear translation of the center of rotation [8]. Figure 5 illustrates this phenomenon.

Symmetry-breaking.

For simulations of (1.4) involving lattice inhomogeneities ($\varepsilon \neq 0$), we typically use as initial condition the $u - v$ state of a homogeneous integration (such as that depicted in Figure 3), and we choose the size of the perturbation terms $|\varepsilon\, g_i|$ small enough so that the wave retains its overall spiral shape, where $|\cdot|$ denotes the uniform norm. For example, in Figure 6, we show the u component of such an inhomogeneous case. The effect of the perturbation on the wave profile can be easily observed.

1.3 Outline of the paper.

The paper is organized as follows. In section 2, we present the functional analytic framework and hypotheses. The goal is to reduce the problem of studying the effects of lattice symmetry-breaking perturbations in (1.2) on relative periodic solutions, to that of studying the asymptotic behavior of solutions of a four-dimensional system of ODEs (2.9) (center

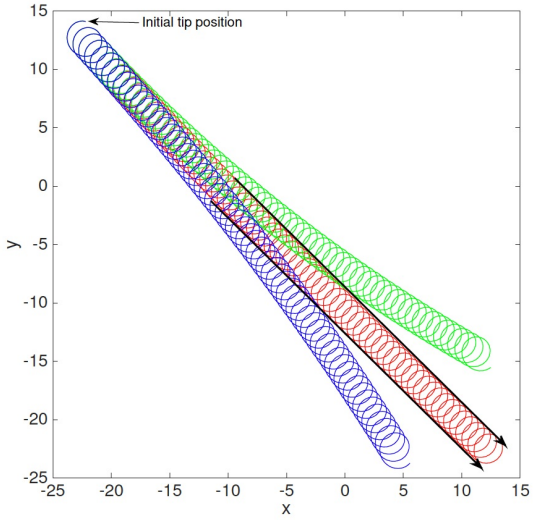

Figure 5: Superposition of meander paths for three simulations of (1.4) with $\varepsilon = 0$ and the same initial condition in all three cases, which illustrate the transition from meandering with inward petals (green) to outward petals (blue) via linear meandering (red). Parameter values are $\tau = 0.26$, $\gamma = 0.5$, and $\beta = 0.793$ (green), $\beta = 0.79275$ (blue), $\beta = 0.792875$ (red). The parallel black arrows on both sides of the red meander path have been added to the figure to guide the eye.

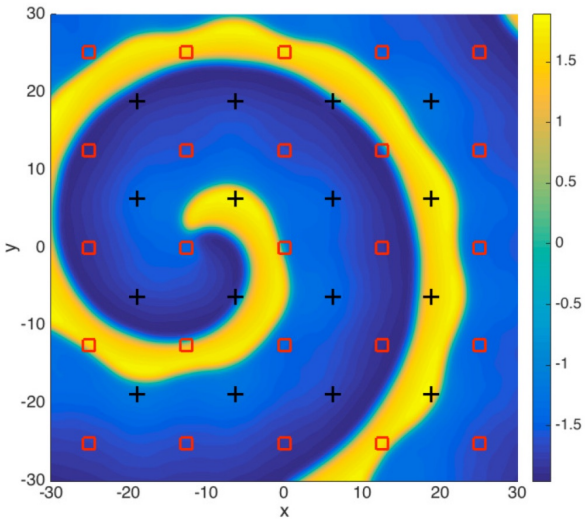

Figure 6: Plot of the u component of an integration of (1.4) with an inhomogeneous perturbation, at a fixed instant in time after transients have dissipated. The effect of the perturbation on the wave profile can be easily observed. The red squares and black crosses represent the lattice and dual lattice, respectively.

bundle equations) possessing symmetry properties related to those of (1.2).

One of our most important analytical tools in this paper is Hale's theory of averaging of multiply periodic differential equations and associated results on the existence of integral manifolds, presented in [19, Theorem 2.3, section VII.2] (see also [40]). In section 3, we perform certain changes of coordinates on (2.9) in order to transform these equations into forms that are suitable for application of Hale's theorem. The analysis also depends on the commensurability or incommensurability of various quantities which will be described later. Furthermore, this is related to the classical problem of small divisors [4, 14], which we briefly summarize in section 4.

Our main results are contained in sections 5, 6, and 7 where we study the effects of lattice symmetry-breaking on, respectively, quasi-periodic meandering waves, meandering waves whose meander path is a closed epicycle (we will pay special attention to phase-locking in this case), and modulated travelling waves. In each of these three sections, we give the main mathematical results, give an interpretation of how these mathematical results translate to dynamical features of spiral waves, and then illustrate with numerical results performed on (1.4) for various choices of inhomogeneity functions g_i and various kinematic parameters τ, β and γ.

We end with a discussion in section 8. Some of the more technical proofs are omitted from the main text and are instead presented in Appendix A.

2 Preliminaries

The special Euclidean group, denoted by $\mathbf{SE}(2)$, is the set of all planar translations and rotations. We parametrize this group as

$$\mathbf{SE}(2) = \{(\phi, p) \in \mathbf{S}^1 \times \mathbb{R}^2\}.$$

The action of an element (ϕ, p) of $\mathbf{SE}(2)$ on a point $z = \begin{pmatrix} x \\ y \end{pmatrix} \in \mathbb{R}^2$, is given by

$$(\phi, p) \cdot z = R_\phi \cdot z + p, \tag{2.1}$$

where

$$R_\phi = \begin{pmatrix} \cos\phi & -\sin\phi \\ \sin\phi & \cos\phi \end{pmatrix}, \; p = \begin{pmatrix} p_x \\ p_y \end{pmatrix}. \tag{2.2}$$

We define Σ to be the following subgroup of $\mathbf{SE}(2)$:

$$\Sigma = \left\{ (\phi, p) \in \mathbf{SE}(2) \,|\, \phi = \frac{n_1\pi}{2} \,(\mathrm{mod}\, 2\pi),\, p = \begin{pmatrix} 2\pi n_2 \\ 2\pi n_3 \end{pmatrix},\; n_1, n_2, n_3 \in \mathbb{Z} \right\}, \tag{2.3}$$

which represents the symmetry subgroup of a regular square lattice.

Let X be a Banach space, and suppose

$$a : \mathbf{SE}(2) \to GL(X)$$

is a faithful and isometric[†] representation of $\mathbf{SE}(2)$ in the space of bounded, invertible linear operators on X. The situation we have in mind is that X is a space of functions defined from $\mathbb{R}^2$ into $\mathbb{R}^N$, and the action a on X is

$$(a(\nu)U)(z) = U(\nu^{-1} \cdot z),\ \nu = (\phi, p) \in \mathbf{SE}(2),\ U \in X,$$

where the dot in this equation denotes the group action defined in (2.1).

We consider a semilinear autonomous differential equation on X of the form

$$w_t = \mathcal{A}w + \mathscr{F}(w) + \varepsilon\mathscr{G}(w, \varepsilon), \tag{2.4}$$

where $\varepsilon \geq 0$ is a small parameter, $\mathcal{A}$, $\mathscr{F}$, and $\mathscr{G}$ are C^k smooth nonlinearities ($k \geq 3$) which satisfy conditions such that (2.4) generates a smooth local semiflow $\Phi_{t,\varepsilon}$ on X [20], and $\mathscr{G}$ is bounded. We will suppose that the degree of smoothness k is large enough to justify the Taylor expansions that we will perform in the paper.

We assume the following hypothesis on the semiflow $\Phi_{t,\varepsilon}$.

Hypothesis 2.1

$$\Phi_{t,0}(a(\nu)w) = a(\nu)\Phi_{t,0}(w) \quad \forall w \in X,\ \nu \in \mathbf{SE}(2),\ t > 0,$$

and for $\varepsilon > 0$, we have

$$\Phi_{t,\varepsilon}(a(\nu)w) = a(\nu)\Phi_{t,\varepsilon}(w) \quad \forall w \in X, \forall t > 0 \iff \nu \in \Sigma.$$

This hypothesis means that $\mathcal{A}+\mathscr{F}$ in (2.4) is $\mathbf{SE}(2)$-equivariant, but $\mathscr{G}$ is only Σ-equivariant. It is in this sense that we say that $\mathscr{G}$ *breaks the* $\mathbf{SE}(2)$ *symmetry of* (2.4).

As mentioned in the introduction, we are interested in how the symmetry-breaking term $\mathscr{G}$ in (2.4) affects the dynamics of meandering waves. Thus, we will need to assume that (2.4) admits such solutions when $\varepsilon = 0$.

[†]Recall that a representation is faithful if its kernel contains only the identity of the group. In other words, a faithful representation is an injective group homomorphism. Also, a mapping between two metric spaces is isometric if it preserves the distances between two elements with respect to the corresponding metrics.

Hypothesis 2.2 *(Existence of normally hyperbolic relative periodic solutions)* There exist $w^\star \in X$, $T > 0$, and $\nu^* \in \mathbf{SE}(2)$ such that

$$\Phi_{T,0}(w^*) = a(\nu^*)w^*,$$

and for all $t \in (0, T)$, we have $\Phi_{t,0}(w^*) \notin \{a(\nu)w^* \,|\, \nu \in \mathbf{SE}(2)\}$. Furthermore, we assume that the set $\{\sigma \in \mathbb{C} \mid |\sigma| \geq 1\}$ is a spectral set for the linearization $a(\nu^*)^{-1}D\Phi_{T,0}(w^\star)$, with projection $P_\star$ such that the generalized eigenspace $E = \text{range}(P_\star)$ is four-dimensional (three dimensions corresponding to the symmetry eigenvalues, and one corresponding to the flow direction).

For simplicity, we will only be interested in one-armed spiral waves, so we assume the isotropy subgroup of $w^\star$ in Hypothesis 2.2 is trivial, i.e.,

$$a(\phi, p) \cdot w^\star = w^\star \iff (\phi, p) = (0, 0).$$

Remark 2.3 The group element $a(\nu^*)$ in Hypothesis 2.2 is either a rotation (around an arbitrary fixed point) or a translation. In the former case, the spiral wave evolves in time in such a way that the tip of the spiral traces out an epicyclic path (with petals either inward or outward): see, for example, [6, 7, 9, 42, 43], which coined such states as *meandering*. Such a state is illustrated in Figure 4. In the case where $a(\nu^*)$ is a translation, the path of the spiral tip is a combination of a rotation superimposed with a translation; the center of rotation travels linearly at a constant speed. These states were described in [8] as occurring arbitrarily close to a point of resonant Hopf bifurcation from a purely rotating spiral wave. See the red meander path of Figure 5 for an illustration of such a state.

We will assume that all other (smoothness) hypotheses of the center manifold theorem of [35, 36] are satisfied:

- $a(g)w^\star$ is C^k smooth in $g \in \mathbf{SE}(2)$;
- for any neighborhood U of the identity in $\mathbf{SE}(2)$, there is a $\delta > 0$ such that

$$g \in U,\ g \neq Id \implies |a(g)w^\star - w^\star|_X \geq \delta;$$

- the operators $a(g)P_\star$ and $P_\star a(g)$ are C^{k-1} smooth in $g \in \mathbf{SE}(2)$ in the operator norm;
- the tangent space at $w^\star$ of the group orbit $\mathbf{SE}(2)\, w^\star$, $T_{w^\star}(\mathbf{SE}(2)\, w^\star)$ is contained in $E = \text{range}(P_\star)$.

As is shown in [36], in the applications of interest to us here, i.e., the case where (2.4) is a planar reaction-diffusion equation, the action of $\mathbf{SE}(2)$ is the standard action on the plane, and $w^\star$ represents a one-armed spiral wave, the above-listed smoothness conditions follow from the spectral hypothesis, Hypothesis 2.2 (see Theorem 6.1 of [36]). Also, in our case, Hypothesis 2.2 implies that the center unstable space $E = \text{range}(P_\star)$ is written as

$$E = T_{w^\star}(\mathbf{SE}(2)\, w^\star) \oplus \text{ span} \left\{ \frac{d}{dt} w^\star(t) \Big|_{t=0} \right\};$$

i.e., the bifurcation space $V_\star$ in formula (2.5) of [36] is trivial, $V_\star = \{0\}$, so that the only neutral eigenvalues are those associated to the symmetry and time-flow directions.

Under all of these assumptions and hypotheses, it follows (see equation (7.1) of [36]) that when $\varepsilon = 0$, (2.4) admits an $\mathbf{SE}(2)$-invariant C^{k-1} smooth semiflow-invariant center manifold $\mathcal{M}_c$, which is diffeomorphic to $\mathbb{R}^2 \times \mathbb{T}^2$ (where $\mathbb{T}^2$ is the two-torus), on which the semiflow reduces to

$$\begin{aligned} \dot{q} &= R_\varphi \tilde{h}_1(\theta) \\ \dot{\varphi} &= \omega_1 + \tilde{h}_2(\theta) \\ \dot{\theta} &= \omega_2, \end{aligned} \tag{2.5}$$

where

$$\begin{pmatrix} q \\ \varphi \\ \theta \end{pmatrix} = \begin{pmatrix} q_1 \\ q_2 \\ \varphi \\ \theta \end{pmatrix} \in \mathcal{M}_c \cong \mathbb{R}^2 \times \mathbb{T}^2,$$

$\tilde{h}_{1,2}$ are C^{k-2} smooth and 2π-periodic in θ, with

$$\langle \tilde{h}_2 \rangle \equiv \frac{1}{2\pi} \int_0^{2\pi} \tilde{h}_2(\theta) d\theta = 0, \tag{2.6}$$

$\omega_1 \geq 0$ and $\omega_2 > 0$ are constant real numbers (rotation frequency and meander frequency, respectively, of the meandering spiral wave), and we remind the reader that R_φ is the rotation matrix (2.2). The action of $\mathbf{SE}(2)$ on the manifold $\mathcal{M}_c \cong \mathbb{R}^2 \times \mathbb{T}^2$ reduces to

$$(\phi, p) \cdot (q, \varphi, \theta) = (R_\phi q + p, \varphi + \phi, \theta), \tag{2.7}$$

and the ODEs (2.5) are invariant with respect to this action. Since $\mathscr{G}$ is bounded on X, then by Hypothesis 2.2, the normally hyperbolic invariant manifold $\mathcal{M}_c$ will persist as a semiflow invariant manifold $\mathcal{M}_c(\varepsilon) \cong \mathcal{M}_c \cong \mathbb{R}^2 \times \mathbb{T}^2$ of (2.4) for all small-enough $\varepsilon > 0$. However, by Hypothesis 2.1, the flow on this manifold will only be Σ-invariant for $\varepsilon > 0$ (via actions

(2.7) and (2.3)). The general form of a Σ-invariant ODE on $\mathbb{R}^2 \times \mathbb{T}^2$, which reduces to (2.5) at $\varepsilon = 0$, is

$$\begin{aligned} \dot{q} &= R_\varphi[\tilde{h}_1(\theta) + \varepsilon\Gamma_1(q,\varphi,\theta,\varepsilon)] \\ \dot{\varphi} &= \omega_1 + \tilde{h}_2(\theta) + \varepsilon\Gamma_2(q,\varphi,\theta,\varepsilon) \\ \dot{\theta} &= \omega_2 + \varepsilon\Gamma_3(q,\varphi,\theta,\varepsilon), \end{aligned} \tag{2.8}$$

where, because of the translational symmetries of the lattice, the C^{k-2} smooth functions Γ_j are 2π-periodic in each of the components of $q \in \mathbb{R}^2$, as well as being 2π-periodic in φ and θ. Because of the periodicity in q, we choose to view (2.8) on a manifold $\mathcal{X}$ which is diffeomorphic to the four-torus $\mathbb{T}^4$:

$$\begin{aligned} \dot{\Psi} &= R_\varphi\left[h_1(\theta) + \varepsilon F_1(\Psi,\varphi,\theta,\varepsilon)\right] \\ \dot{\varphi} &= \omega + h_2(\theta) + \varepsilon F_2(\Psi,\varphi,\theta,\varepsilon) \\ \dot{\theta} &= 1, \end{aligned} \tag{2.9}$$

where time has been rescaled along the orbits to set the $\dot{\theta}$ equation to 1, and the variables $\Psi = (\psi_1, \psi_2)$ are the translation variables q of the center manifold equations (2.8), but viewed modulo the lattice of the perturbation. When one of the variables $\psi_{1,2}$ advances through a complete period of 2π, this should be interpreted in physical space as the spiral having advanced to a neighboring fundamental domain in the spatial grid. The variables φ and θ are the two phases of the quasi-periodic meandering spiral. Because there has been a rescaling of time to set the coefficient of the $\dot{\theta}$ equation in (2.9) to 1, the coefficient ω in (2.9) in fact represents a ratio of the two frequencies of the epicyclic meandering in (2.4) when $\varepsilon = 0$.

In (2.9), the C^{k-2} functions $F_{1,2}$ satisfy the additional discrete rotational (by $\pi/2$) symmetry

$$F_{1,2}\left(-J\Psi, \varphi + \frac{\pi}{2}, \theta, \varepsilon\right) = F_{1,2}(\Psi,\varphi,\theta,\varepsilon) \;\; \forall \begin{pmatrix} \Psi \\ \varphi \\ \theta \end{pmatrix} \in \mathbb{T}^4, \; 0 \le \varepsilon \ll 1, \tag{2.10}$$

where

$$J \equiv R_{-\frac{\pi}{2}} = \begin{pmatrix} 0 & 1 \\ -1 & 0 \end{pmatrix}.$$

The group $\mathbf{SE}(2)$ acts on the phase space $\mathcal{X} = \mathbb{T}^4$ of (2.9) as follows:

$$(\phi, p) \cdot \begin{pmatrix} \Psi \\ \varphi \\ \theta \end{pmatrix} = \begin{pmatrix} (R_\phi \Psi + p) \,(\mathrm{mod}\,[0,2\pi] \times [0,2\pi]) \\ \varphi + \phi \;(\mathrm{mod}\, 2\pi) \\ \theta \end{pmatrix}.$$

When $\varepsilon = 0$, (2.9) is equivariant with respect to this action. However, when $\varepsilon > 0$, property (2.10) implies that the lattice subgroup Σ, defined in (2.10), is the symmetry group of (2.9). Thus, (2.9) reflects the forced symmetry-breaking property of (2.4). When $\varepsilon > 0$, if $(\Psi(t), \varphi(t), \theta(t))$ is a solution of (2.9), then so is $\big(J\Psi(t), \varphi(t) - \frac{\pi}{2}, \theta(t)\big)$.

We end this section with a remark.

Remark 2.4 The functions $F_{1,2}$, $h_{1,2}$ and the number ω in (2.9) obviously depend on the operator $\mathcal{A}$ and the functions $\mathscr{F}$ and $\mathscr{G}$ in (2.4) via the center manifold reduction process. By studying, as we do in this paper, generic properties of the class of ODEs of the general form (2.9) without further specifications, we are in a sense studying the range of possible generic local dynamics near relative periodic solutions of the infinite-dimensional system (2.4). However, as a practical consideration, one would like to be able to obtain a formula that maps between the space of functions $\mathcal{A}$, $\mathscr{F}$, and $\mathscr{G}$ in (2.4), and the space of functions $F_{1,2}$, $h_{1,2}$ and the number ω in (2.9). This is a very difficult problem in general and requires information which is usually not readily available, for example, an explicit algebraic representation of the unperturbed meandering spiral wave solution (note, however, that some recent progress has been made in making this link between perturbations at the PDE level and perturbations in the dynamics of reduced center manifold systems, see [39]). With this limitation in mind, our goals in this paper will be more modest. We will characterize certain model-independent features of solutions to system (2.9) and interpret these results in terms of how a weak lattice symmetry-breaking perturbation generically affects the dynamics of relative periodic solutions of (2.4).

3 Preparing the ODEs (2.9) for averaging

In the previous section, we saw that the local dynamics of (2.4) near the relative periodic solution reduces to the center bundle ODEs (2.9) defined on the four-torus $\mathbb{T}^4$, where the function $h_2(\theta)$ satisfies the zero-mean condition (2.6).

Later in the paper, we will want to apply results from the theory of averaging and integral manifolds, as set forth in [19], to find invariant periodic solutions and invariant tori to (2.9) for small $\varepsilon > 0$. For a more modern treatment, the reader may also refer to [40].

Recall that Hale's theorem applies to ODEs of the form

$$\begin{aligned} \dot{X} &= \varepsilon A X + \varepsilon F(\Phi, X, \varepsilon) \\ \dot{\Phi} &= \omega + \varepsilon \Theta(\Phi, X, \varepsilon), \end{aligned} \tag{3.1}$$

where $X \in \mathbf{R}^n$, $\Phi \in \mathbf{R}^m$, $\omega \in \mathbf{R}^m$ is a constant vector, and A is an n by n matrix of constants

of block diagonal form

$$A = \left(\begin{array}{c|c} A_s & 0 \\ \hline 0 & A_u \end{array} \right),$$

where A_s has all eigenvalues with negative real part and A_u has all eigenvalues with positive real part.

Theorem 3.1 *([19, § VII.2, Theorem 2.3])*
Consider the system (3.1), and define

$$\Omega(r_0, \varepsilon_0) = \{(X, \varepsilon) : |X| < r_0, 0 \leq \varepsilon \leq \varepsilon_0\}.$$

Suppose that Θ, F satisfy the following conditions:

(C1) *Θ and F are continuous and bounded in $\mathbf{R}^m \times \Omega(r_0, \varepsilon_0)$.*

(C2) *Θ and F are Lipschitz in Φ in $\mathbf{R}^m \times \Omega(r, \varepsilon)$, with Lipschitz constants $L_\Phi^\Theta(r, \varepsilon)$ and $L_\Phi^F(r, \varepsilon)$ respectively, where $L_\Phi^\Theta(r, \varepsilon)$, $L_\Phi^F(r, \varepsilon)$ are continuous and nondecreasing for $0 \leq r \leq r_0$, $0 \leq \varepsilon \leq \varepsilon_0$, and $L_\Phi^F(0, 0) = 0$.*

(C3) *Θ and F are Lipschitz in X with Lipschitz constants $L_X^\Theta(r, \varepsilon)$ and $L_X^F(r, \varepsilon)$, respectively, in $\mathbf{R}^m \times \Omega(r, \varepsilon)$, where $L_X^\Theta(r, \varepsilon)$, $L_X^F(r, \varepsilon)$ are continuous and nondecreasing for $0 \leq r \leq r_0$, $0 \leq \varepsilon \leq \varepsilon_0$, and $L_X^F(0, 0) = 0$.*

(C4) *The function $|F(\Phi, 0, \varepsilon)|$ is bounded by $N(\varepsilon)$ for $\Phi \in \mathbf{R}^m$, $0 \leq \varepsilon \leq \varepsilon_0$, where $N(\varepsilon)$ is continuous and nondecreasing for $0 \leq \varepsilon \leq \varepsilon_0$, and $N(0) = 0$.*

Furthermore, since the matrix A has all eigenvalues bounded away from the imaginary axis, there exist $\alpha > 0$, $K > 0$ such that for any real number τ,

$$\begin{aligned} |e^{(t-\tau)\varepsilon A_s}| &\leq K e^{-\varepsilon\alpha(t-\tau)}, \quad t \geq \tau, \\ |e^{(t-\tau)\varepsilon A_u}| &\leq K e^{-\varepsilon\alpha(t-\tau)}, \quad t \leq \tau. \end{aligned}$$

Suppose that $\alpha - \limsup_{\varepsilon \to 0} L_\Phi^\Theta(0, \varepsilon) > 0$.

Then the following conclusions are true for the system (3.1): there exist $\varepsilon_1 > 0$ and continuous functions $D(\varepsilon)$, $\Delta(\varepsilon)$, $0 < \varepsilon \leq \varepsilon_1$, which approach zero as $\varepsilon \to 0$, and a continuous function

$$\sigma : \mathbf{R}^m \times (0, \varepsilon_1] \longmapsto \mathbf{R}^n$$

with $\sigma(\Phi, \varepsilon)$ bounded by $D(\varepsilon)$, Lipschitz in Φ with Lipschitz constant $\Delta(\varepsilon)$, such that the set

$$S_\varepsilon = \{(\Phi, X) : X = \sigma(\Phi, \varepsilon), \Phi \in \mathbf{R}^m\}$$

is an invariant set for the system (3.1). If the functions Θ and F in (3.1) are multiply periodic in Φ with period vector $(T_1, \ldots, T_m)$, then $\sigma(\Phi, \varepsilon)$ is also multiply periodic in Φ with period vector $(T_1, \ldots, T_m)$. Finally, the asymptotic stability of the invariant set S_ε is the same as that of the trivial equilibrium point of the equation $\dot{y} = Ay$.

In order to use this theorem, will need to transform (2.9) into the suitable form (3.1). As will become evident later, the transformations and the resulting transformed system will depend on whether or not ω is an integer in (2.9).

Proposition 3.2 *Suppose ω in (2.9) is not an integer. Then under a suitable change of variables, the system (2.9) is equivalent to*

$$\begin{aligned} \dot{\Psi} &= \varepsilon R_\varphi G_1(\Psi, \varphi, \theta, \varepsilon) \\ \dot{\varphi} &= \omega + \varepsilon G_2(\Psi, \varphi, \theta, \varepsilon) \\ \dot{\theta} &= 1, \end{aligned} \tag{3.2}$$

where $G_{1,2}$ are smooth, 2π-periodic in ψ_1, ψ_2, φ, and θ, and satisfy the lattice symmetry properties (2.10).

Proposition 3.3 *Suppose ω in (2.9) is an integer. Then, under a suitable change of variables, the system (2.9) is equivalent to*

$$\begin{aligned} \dot{\Psi} &= R_\varphi V + \varepsilon R_\varphi H_1(\Psi, \varphi, \theta, \varepsilon) \\ \dot{\varphi} &= \varepsilon H_2(\Psi, \varphi, \theta, \varepsilon) \\ \dot{\theta} &= 1, \end{aligned} \tag{3.3}$$

where $V \in \mathbb{R}^2$ is a constant (which is generically nonzero), and $H_{1,2}$ are smooth, 2π-periodic in ψ_1, ψ_2, φ and θ, and satisfy the lattice symmetry properties (2.10).

The proofs of these propositions are found in Appendix A. In the remainder of this paper, we will analyze systems (3.2) and (3.3) using Theorem 3.1. Since the technical conditions required on the vector field in order to apply this theorem are related to Lipschitz continuity, and we have assumed C^{k-2} smoothness for $k \geq 3$ large enough, then it is fairly straightforward to verify that the hypotheses of Theorem 3.1 will be satisfied for our purposes.

It is well known [4, 14] that an important technical obstacle to transforming a system such as (3.2) or (3.3) into a form similar to (3.1) is the problem of small divisors and resonance manifolds. In the next section, we will briefly address this issue.

4 Small divisors

The problem of *small divisors* is a classical one in the analysis of multiply periodic dynamical systems and is related to solving a linear PDE of the form

$$\omega_1 \frac{\partial r}{\partial \phi_1} + \cdots + \omega_n \frac{\partial r}{\partial \phi_n} = s(\phi_1, \ldots, \phi_n)$$

by way of a multiple Fourier series

$$r(\phi_1, \ldots, \phi_n) = \sum_{(m_1,\ldots,m_n)\in\mathbb{Z}^n} A_{m_1,\ldots,m_n}\, e^{i(m_1\phi_1+\cdots+m_n\phi_n)}$$

given $s(\phi_1, \ldots, \phi_n) = \sum_{(m_1,\ldots,m_n)\in\mathbb{Z}^n} B_{m_1,\ldots,m_n}\, e^{i(m_1\phi_1+\cdots+m_n\phi_n)}$ with $B_{0,\ldots,0} = 0$. Formal integration of the PDE leads to

$$A_{m_1,\ldots,m_n} = \frac{B_{m_1,\ldots,m_n}}{i(m_1\omega_1 + \cdots + m_n\omega_n)},\ (m_1, \ldots, m_n) \in \mathbb{Z}^n \setminus \{(0, \ldots, 0)\},$$

where the denominator can get arbitrarily small even if $\omega_1, \ldots, \omega_n$ are linearly independent over the rationals. So we cannot guarantee the convergence of the series for r, (unless s is a trigonometric polynomial, in which case convergence is not an issue). We must thus impose restrictions on $\omega_1, \ldots, \omega_n$ in the process of solving the above PDE using Fourier series.

Definition 4.1 *A vector* $\mathbf{\Omega} = (\omega_1, \ldots, \omega_n) \in \mathbb{R}^n$, $n \in \mathbb{N}$, *is said to satisfy a* diophantine condition of constant $\rho > 0$ and exponent $\mu \geq n - 1$, *and we write* $\mathbf{\Omega} \in C_{\rho,\mu}$, *if for every* $\mathbf{m} = (m_1, \ldots, m_n) \in \mathbb{Z}^n$, *we have*

$$|\langle \mathbf{m}, \mathbf{\Omega} \rangle| \equiv \left| \sum_{j=1}^{n} m_j \omega_j \right| \geq \rho |\mathbf{m}|^{-\mu},$$

where $|\mathbf{m}| = \sum_{j=1}^{n} |m_j|$.

One can show [14] that the Lebesgue measure of $C_{\rho,\mu}$ is positive.

The following is an adaptation of Theorem 12.9 of [14], where we also use well-known results on the rate of convergence of Fourier coefficients and the degree of smoothness of the corresponding Fourier series [31].

Proposition 4.2 *Suppose* $\mathbf{\Omega} = (\omega_1, \ldots, \omega_n) \in \mathbb{R}^n$ *is such that its components are linearly independent over the rationals, and consider the PDE on the torus* $\mathbb{T}^n$,

$$\sum_{k=1}^{n} \omega_k \frac{\partial r}{\partial \phi_k}(\mathbf{x}, \phi_1, \ldots, \phi_n) = s(\mathbf{x}, \phi_1, \ldots, \phi_n) \tag{4.1}$$

where $\mathbf{x} \in K \subset \mathbb{R}^q$, *and* K *is compact.*

(a) If $s(\mathbf{x},\boldsymbol{\phi}) = s(\mathbf{x},\phi_1,\ldots,\phi_n)$ is a trigonometric polynomial of the form

$$s(\mathbf{x},\boldsymbol{\phi}) = \sum_{m_1=-N_1}^{N_1} \cdots \sum_{m_n=-N_1}^{N_1} B_{\mathbf{m}}(\mathbf{x}) e^{i\langle \mathbf{m},\boldsymbol{\phi}\rangle}$$

with $B_{\mathbf{0}} = 0$, then the trigonometric polynomial

$$r(\mathbf{x},\boldsymbol{\phi}) = \sum_{m_1=-N_1}^{N_1} \cdots \sum_{m_n=-N_1}^{N_1} A_{\mathbf{m}}(\mathbf{x}) e^{i\langle \mathbf{m},\boldsymbol{\phi}\rangle},$$

where $A_{\mathbf{0}} = 0$ and $A_{\mathbf{m}}(\mathbf{x}) = \frac{B_{\mathbf{m}}(\mathbf{x})}{i\langle \mathbf{m},\boldsymbol{\Omega}\rangle}$, $\mathbf{m} \neq \mathbf{0}$, is a solution to (4.1).

(b) If $s(\mathbf{x},\boldsymbol{\phi}) = \sum_{\mathbf{m}\in\mathbb{Z}^n} B_{\mathbf{m}}(\mathbf{x}) e^{i\langle \mathbf{m},\boldsymbol{\phi}\rangle}$ (with $B_{\mathbf{0}} = \mathbf{0}$) is smooth but not a trigonometric polynomial, and if $\boldsymbol{\Omega} \in C_{\rho,\mu}$ (for some $\rho > 0$ and $\mu \geq n-1$), then the function

$$r(\mathbf{x},\boldsymbol{\phi}) = \sum_{\mathbf{m}\in\mathbb{Z}^n\setminus\{\mathbf{0}\}} \frac{B_{\mathbf{m}}(\mathbf{x})}{i\langle \mathbf{m},\boldsymbol{\Omega}\rangle} e^{i\langle \mathbf{m},\boldsymbol{\phi}\rangle}$$

is smooth (with degree of smoothness determined by μ) and is a solution to (4.1).

5 The case where ω is irrational in (3.2)

Performing the near identity change of variables $\Psi = \hat{\Psi} + \varepsilon r(\hat{\Psi},\varphi,\theta)$ transforms (3.2) into (upon dropping the hats)

$$\begin{aligned} \dot{\Psi} &= \varepsilon \mathcal{G}(\Psi) + \varepsilon \left[s(\Psi,\varphi,\theta) - \omega \tfrac{\partial r}{\partial \varphi}(\Psi,\varphi,\theta) - \tfrac{\partial r}{\partial \theta}(\Psi,\varphi,\theta) \right] + \varepsilon^2 R_\varphi G_3(\Psi,\varphi,\theta,\varepsilon) \\ \dot{\varphi} &= \omega + \varepsilon G_4(\Psi,\varphi,\theta,\varepsilon) \\ \dot{\theta} &= 1, \end{aligned} \tag{5.1}$$

where

$$\mathcal{G}(\Psi) = \frac{1}{(2\pi)^2} \int_{\mathbb{T}^2} R_\varphi G_1(\Psi,\varphi,\theta,0)\, d\varphi d\theta, \tag{5.2}$$

and

$$s(\Psi,\varphi,\theta) = R_\varphi G_1(\Psi,\varphi,\theta,0) - \mathcal{G}(\Psi). \tag{5.3}$$

The following is a straightforward consequence of Proposition 4.2.

Proposition 5.1 *If s in (5.1) and (5.3) is a trigonometric polynomial, or if $\mathbf{\Omega} = (\omega, 1) \in C_{\rho,\mu}$ as defined in Definition 4.1, then a smooth function r can be found so that (5.1) simplifies to*

$$\begin{aligned} \dot{\Psi} &= \varepsilon \mathcal{G}(\Psi) + \varepsilon^2 R_\varphi G_3(\Psi, \varphi, \theta, \varepsilon) \\ \dot{\varphi} &= \omega + \varepsilon G_4(\Psi, \varphi, \theta, \varepsilon) \\ \dot{\theta} &= 1, \end{aligned} \tag{5.4}$$

where $\mathcal{G}$ is as in (5.2). Moreover, $G_{3,4}$ satisfy the symmetry properties (2.10), and $\mathcal{G}(J\Psi) = J\mathcal{G}(\Psi)$, i.e., $\mathcal{G}$ is J-equivariant.

The two-dimensional J-equivariant system

$$\dot{\Psi} = \varepsilon\, \mathcal{G}(\Psi) \tag{5.5}$$

has an equilibrium at $\Psi = 0$, and any nontrivial equilibria occur as a conjugate set

$$\left\{ J^k \Psi^\star,\ k = 0, 1, 2, 3 \right\}.$$

If $\{\Psi(t) |\ 0 \le t \le T\}$ is a T-periodic orbit of (5.5), then either $\left\{ J^k \Psi(t) |\ 0 \le t \le T \right\}$ is a distinct periodic orbit for $k = 1, 2, 3$ or $\{J\Psi(t) |\ 0 \le t \le T\}$ coincides with the orbit $\{\Psi(t) |\ 0 \le t \le T\}$. In this latter case, the periodic solution has one of the following spatial-temporal symmetries: [17]

$$\Psi(t - T/4) = \pm J\Psi(t). \tag{5.6}$$

The main result of this section is the following theorem.

Theorem 5.2 *Let us consider* (5.5).

(i) Suppose (5.5) *has an equilibrium at $\Psi^\star$ which is linearly stable (resp. unstable). Then for $\varepsilon > 0$ small enough, the system* (5.4) *has linearly stable (resp. unstable) invariant two-tori represented as*

$$\Psi = J^k \left(\Psi^\star + \sqrt{\varepsilon} \sigma_{\Psi^\star} \left(\varphi + \frac{k\pi}{2}, \theta, \varepsilon \right) \right),\ k = 0, 1, 2, 3, \tag{5.7}$$

where the smooth function $\sigma_{\Psi^\star}$ is such that $\sigma_{\Psi^\star} \to 0$ as $\varepsilon \to 0$. If $\Psi^\star = 0$, then the torus has the $\mathbb{Z}_4$-symmetry

$$\sigma_0 \left(\varphi - \frac{\pi}{2}, \theta, \varepsilon \right) = J\sigma_0(\varphi, \theta, \varepsilon). \tag{5.8}$$

(ii) Suppose $\{\Psi^\star(t)|\ 0 \le t \le T\}$ *is a nontrivial periodic orbit of* (5.5) *and that this orbit is linear stable (resp., unstable). Then for* $\varepsilon > 0$ *small enough, the system* (5.4) *has linearly stable (resp., unstable) invariant three-tori represented as*

$$\begin{array}{l} \Psi = J^k\left(\Psi^\star(\eta + kT/4) \quad + \sqrt{\varepsilon}\,\Sigma_{\Psi^\star}\left(\eta + kT/4, \varphi + k\pi/2, \theta, \varepsilon\right)\right),\ k = 0,1,2,3, \\ \qquad\qquad (\eta, \varphi, \theta) \in [0,T] \times [0, 2\pi] \times [0, 2\pi], \end{array} \tag{5.9}$$

where the smooth function $\Sigma_{\Psi^\star}$ *is such that* $\Sigma_{\Psi^\star} \to 0$ *as* $\varepsilon \to 0$. *Furthermore, if* $\Psi^\star$ *satisfies the spatial-temporal symmetry* (5.6)*, then the invariant three-torus is such that*

$$\Sigma_{\Psi^\star}(\eta - T/4, \varphi \mp \pi/2, \theta, \varepsilon) = \pm J \Sigma_{\Psi^\star}(\eta, \varphi, \theta, \varepsilon). \tag{5.10}$$

Proof We first prove item (i). Setting

$$\Psi = \Psi^* + \sqrt{\varepsilon}\hat{\Psi} \tag{5.11}$$

transforms (5.4) into the following (upon dropping the hats):

$$\begin{array}{rcl} \dot{\Psi} &=& \varepsilon D_\Psi \mathcal{G}(\Psi^*)\Psi + \varepsilon^{\frac{3}{2}} R_\varphi \mathcal{R}_1(\Psi, \varphi, \theta, \varepsilon) \\ \dot{\varphi} &=& \omega + \varepsilon \mathcal{R}_2(\Psi, \varphi, \theta, \varepsilon) \\ \dot{\theta} &=& 1, \end{array} \tag{5.12}$$

where $\mathcal{R}_{1,2}$ are smooth and 2π-periodic in φ and in θ. System (5.12) is in the appropriate form to apply Theorem 3.1, and we conclude that (5.12) has an invariant two-torus of the form $\Psi = \sigma_{\Psi^*}(\varphi, \theta, \varepsilon)$ for all $\varepsilon > 0$ sufficiently small, with $\sigma_{\Psi^*} \to 0$ as $\varepsilon \to 0$. Using (5.11), we get that (5.7) with $k = 0$ is an invariant two-torus for (5.4).

For the conjugate equilibrium $J\Psi^*$ of (5.5), we replace (5.11) by

$$\Psi = J(\Psi^* + \sqrt{\varepsilon}\hat{\Psi}).$$

Setting $\varphi = \hat{\varphi} - \pi/2$ and using the equivariance properties of $\mathcal{R}_1$ and $\mathcal{R}_2$, (5.4) also transforms into (5.12) upon dropping the hats. Therefore, $\Psi = J\Psi^* + J\sqrt{\varepsilon}\sigma_{\Psi^*}(\varphi + \pi/2, \theta, \varepsilon)$ is also an invariant two-torus for (5.4) which is distinct from the previous one if $\Psi^* \neq 0$, but if $\Psi^* = 0$, we get (5.8). This ends the proof of item (i).

To prove (ii), we introduce a local orthonormal coordinate system (b, η) near the periodic orbit (see Chapter VI of [19], equations (1.5)-(1.9) for details, and also [12]) defined by

$$\Psi = \Psi^*(\eta) + b\, J \frac{\dot{\Psi}^*(\eta)}{||\dot{\Psi}^*(\eta)||}, \tag{5.13}$$

which transforms (5.4) into

$$\begin{aligned}
\dot{b} &= \varepsilon A(\eta, b)b + \varepsilon^2 \mathcal{U}(b, \eta, \varphi, \theta, \varepsilon) \\
\dot{\eta} &= \varepsilon(1 + B(\eta, b)b) + \varepsilon^2 \mathcal{V}(b, \eta, \varphi, \theta, \varepsilon) \\
\dot{\varphi} &= \omega + \varepsilon \mathcal{W}(b, \eta, \varphi, \theta, \varepsilon) \\
\dot{\theta} &= 1,
\end{aligned} \tag{5.14}$$

where A, B, $\mathcal{U}$, $\mathcal{V}$, and $\mathcal{W}$ are smooth, T-periodic in η, and 2π-periodic in φ and θ, and where

$$A(\eta, 0) = \text{trace}(D_\Psi \mathcal{G}(\Psi^*(\eta))) - \frac{d}{d\eta} \ln(||\dot{\Psi}^*(\eta)||).$$

If we define

$$\delta = \frac{1}{T} \int_0^T A(s, 0)\, ds = \frac{1}{T} \int_0^T \text{trace}(D_\Psi \mathcal{G}(\Psi^*(s)))\, ds,$$

then $\delta < 0$ (resp., $\delta > 0$) if the limit cycle $\Psi^*(t)$ is linearly stable (resp., unstable). Substituting the periodic change of variable

$$b = \sqrt{\varepsilon}\, \xi e^{\int_0^\eta (A(s,0) - \delta)\, ds} \tag{5.15}$$

into (5.14) yields

$$\begin{aligned}
\dot{b} &= \sqrt{\varepsilon}\, \dot{\xi} e^{\int_0^\eta (A(s,0)-\delta)\, ds} + \sqrt{\varepsilon}\, \xi e^{\int_0^\eta (A(s,0)-\delta)\, ds} (A(\eta, 0) - \delta)\dot{\eta} \\
&= \varepsilon A(\eta, \sqrt{\varepsilon}\, \xi e^{\int_0^\eta (A(s,0)-\delta)\, ds}) \sqrt{\varepsilon}\, \xi e^{\int_0^\eta (A(s,0)-\delta)\, ds} + \varepsilon^2 \mathcal{U}(\sqrt{\varepsilon}\, \xi e^{\int_0^\eta (A(s,0)-\delta)\, ds}, \eta, \varphi, \theta, \varepsilon),
\end{aligned}$$

from which it follows that

$$\begin{aligned}
&\dot{\xi} + \xi\, (A(\eta, 0) - \delta)(\varepsilon\, (1 + B(\eta, \sqrt{\varepsilon}\, \xi e^{\int_0^\eta (A(s,0)-\delta)\, ds})\, \sqrt{\varepsilon}\, \xi e^{\int_0^\eta (A(s,0)-\delta)\, ds}) + \\
&\varepsilon^2\, \mathcal{V}(\sqrt{\varepsilon}\, \xi e^{\int_0^\eta (A(s,0)-\delta)\, ds}, \eta, \varphi, \theta, \varepsilon)) \\
&= \varepsilon A(\eta, \sqrt{\varepsilon}\, \xi e^{\int_0^\eta (A(s,0)-\delta)\, ds})\, \xi + \varepsilon^{3/2} \mathcal{U}(\sqrt{\varepsilon}\, \xi e^{\int_0^\eta (A(s,0)-\delta)\, ds}, \eta, \varphi, \theta, \varepsilon) e^{-\int_0^\eta (A(s,0)-\delta)\, ds}.
\end{aligned}$$

Performing Taylor expansions and renaming functions leads to

$$\begin{aligned}
\dot{\xi} &= \varepsilon\delta\xi + \varepsilon^{\frac{3}{2}} U(\xi, \eta, \varphi, \theta, \varepsilon) \\
\dot{\eta} &= \varepsilon + \varepsilon^{\frac{3}{2}} V(\xi, \eta, \varphi, \theta, \varepsilon) \\
\dot{\varphi} &= \omega + \varepsilon W(\xi, \eta, \varphi, \theta, \varepsilon) \\
\dot{\theta} &= 1,
\end{aligned} \tag{5.16}$$

which is in the proper form to apply Theorem 3.1, and we conclude that (5.16) admits an invariant three-torus

$$\xi = \sigma_{\Psi^*}(\eta, \varphi, \theta, \varepsilon), \quad \sigma_{\Psi^*} \to 0, \text{ as } \varepsilon \to 0.$$

Using (5.13), we conclude that (5.4) admits an invariant three-torus

$$\Psi = \Psi^*(\eta) + \sqrt{\varepsilon}\Sigma_{\Psi^*}(\eta, \varphi, \theta, \varepsilon),$$

where

$$\Sigma_{\Psi*}(\eta, \varphi, \theta, \varepsilon) = \sigma_{\Psi^*}(\eta, \varphi, \theta, \varepsilon) e^{\int_0^\eta (A(s,0)-\delta)\, ds} \frac{J\dot{\Psi}^*(\eta)}{||\dot{\Psi}^*(\eta)||}.$$

We have thus established (5.9) in the case $k = 0$. The other cases for k in (5.9) and the spatiotemporal symmetry property (5.10) follow using arguments similar to those used in the proof of item (i) above. ∎

Interpretation. Two-frequency meandering spiral waves have been observed in RDPDE systems such as (1.4) when $\varepsilon = 0$ [8]. If the two frequencies are incommensurate, then the meander path typically resembles that in Figure 4, and this path densely fills a circular annulus. Theorem 5.2 characterizes the simplest ways in which these meandering waves typically behave under a generic lattice symmetry-breaking perturbation, assuming the frequency ratio satisfies a Diophantine condition.

One possibility is that the two-frequency meandering wave drifts and anchors at a point in space that may or may not be a lattice point. If the point of anchoring is a point of the lattice, then the meander path will typically lose the full circular symmetry of Figure 4 but retains a fourfold rotational symmetry. If the point of anchoring is not related to the lattice, then we expect that the meander path will not retain any rotational symmetries. Furthermore, to any such anchored meander paths, there are conjugate anchored meander paths related to the first one by the symmetries of the lattice.

Another possibility is that the lattice symmetry-breaking induces a third (slow) frequency in the meandering motion of the spiral. Again, the resultant three-frequency motion will be anchored at some point in space. If this anchoring point is a lattice point, then the three-frequency meander path has overall fourfold rotational symmetry, otherwise it retains no rotational symmetries. Again, lattice symmetries lead to conjugate three-frequency meandering states.

In Figures 7 and 8, we show the meander path of a spiral wave solution observed in a numerical simulations of (1.4) with inhomogeneity data (1.5) given, respectively, by

$$\varepsilon = 0.01,\ A_1 = -0.7,\ A_2 = 0.14,\ B_1 = -2.5,\ B_2 = -0.5,\ C_1 = 0.5,\ C_2 = 1.5 \text{ for Figure 7} \tag{5.17}$$

and

$$\varepsilon = 0.01,\ A_1 = -0.9,\ A_2 = 0.46,\ B_1 = -2.5,\ B_2 = 0.5,\ C_1 = -0.5,\ C_2 = 1.5 \text{ for Figure 8.} \tag{5.18}$$

We have chosen the same kinetic parameters $\tau = 0.1858$, $\beta = 0.755$, $\gamma = 0.5$ as for the simulation of the fully Euclidean case illustrated in Figure 4. After transients have died out, one observes a two-frequency meandering wave which is anchored at a point that is not a lattice point in Figure 7, and a three-frequency meandering wave which is anchored at a lattice point in Figure 8.

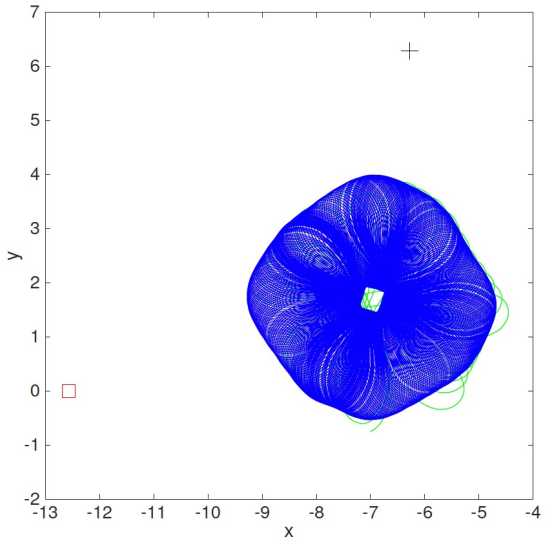

Figure 7: A two-frequency anchored meandering path for a spiral wave in (1.4) with inhomogeneity data (5.17) and kinetic parameters $\tau = 0.1858$, $\beta = 0.755$, $\gamma = 0.5$. The red square and black cross are there for reference purposes to illustrate points of the lattice and the dual lattice, respectively. The transient is in green, and the final anchored state is in blue.

6 The case where ω is rational and non-integer in (3.2)

When $\omega = k/\ell$ is rational (but not an integer) in (3.2) (with $\gcd(k, \ell) = 1$), then, as we will see in this section, phase-locking of meandering waves can occur. We prepare (3.2) for

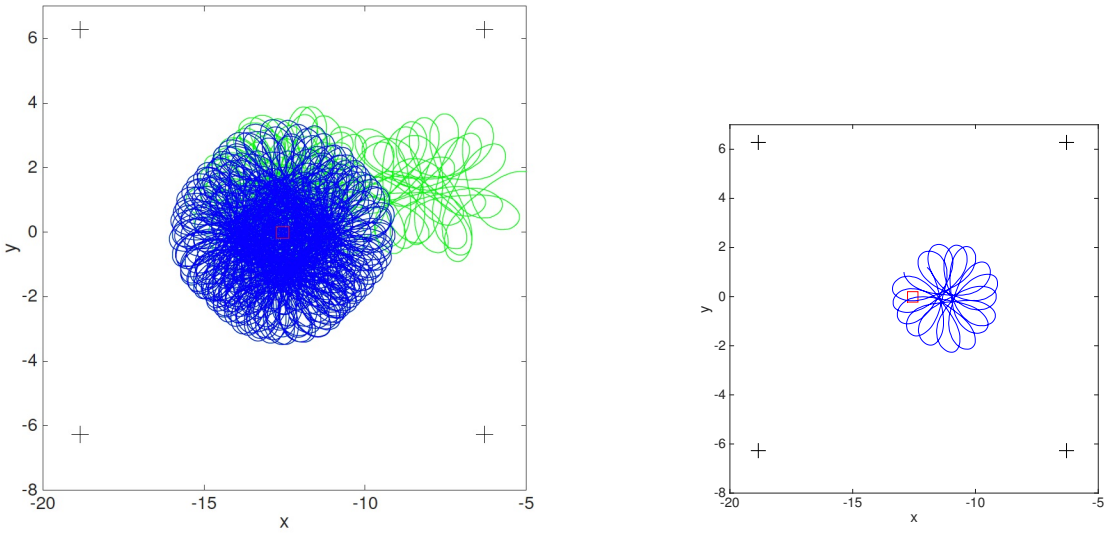

Figure 8: On the left: A three-frequency anchored meandering path for a spiral wave in (1.4) with inhomogeneity data (5.18) and kinetic parameters $\tau = 0.1858$, $\beta = 0.755$, $\gamma = 0.5$. The red square and black crosses are there for reference purposes to illustrate points of the lattice and the dual lattice, respectively. The transient is in green, and the final anchored state is in blue. On the right we show only a portion (limited in time) of the blue meander path from the left figure. We can see that on this small time interval, the motion is approximately two-frequency epicyclic. The third (slower) frequency moves this basic two-frequency meander path around the red square (lattice point), producing the overall blue meander path seen in the left figure.

averaging by setting $\hat{\varphi} = \varphi - k\theta/\ell$, which yields (after dropping the hats)

$$\begin{aligned} \dot{\Psi} &= \varepsilon R_\varphi R_{k\theta/\ell} G_1(\Psi, \varphi + k\theta/\ell, \theta, \varepsilon) \\ \dot{\varphi} &= \varepsilon G_2(\Psi, \varphi + k\theta/\ell, \theta, \varepsilon) \\ \dot{\theta} &= 1. \end{aligned} \tag{6.1}$$

We then define the averages

$$\begin{aligned} \mathcal{G}_1(\Psi, \varphi) &= \frac{1}{2\pi\ell} \int_0^{2\pi\ell} R_\varphi R_{k\theta/\ell} G_1(\Psi, \varphi + k\theta/\ell, \theta, 0)\, d\theta \\ \mathcal{G}_2(\Psi, \varphi) &= \frac{1}{2\pi\ell} \int_0^{2\pi\ell} G_2(\Psi, \varphi + k\theta/\ell, \theta, 0)\, d\theta. \end{aligned} \tag{6.2}$$

The following is a straightforward consequence of the standard (singly periodic) theory of averaging [18, 19, 40]

Theorem 6.1 *Let (Ψ_0, φ_0) be a hyperbolic equilibrium point of the averaged equations*

$$\begin{aligned} \dot{\Psi} &= \varepsilon \mathcal{G}_1(\Psi, \varphi) \\ \dot{\varphi} &= \varepsilon \mathcal{G}_2(\Psi, \varphi). \end{aligned} \tag{6.3}$$

Then for all small enough $\varepsilon > 0$, the system (6.1) has a $2\pi\ell$-periodic solution represented as

$$\Psi = f^1_{(\Psi_0, \varphi_0)}(\theta, \varepsilon), \quad \varphi = f^2_{(\Psi_0, \varphi_0)}(\theta, \varepsilon) \tag{6.4}$$

which tend to Ψ_0 and φ_0, respectively, when $\varepsilon \to 0$. Furthermore, the stability of the periodic solution is the same as the stability of the equilibrium point (Ψ_0, φ_0) in (6.3).

Interpretation. Theorem 6.1 implies that if (Ψ_0, φ_0) is a linearly stable equilibrium point for (6.3), then (6.1) has an asymptotically stable $2\pi\ell$-periodic solution

$$(\Psi(t), \varphi(t)) = (f^1_{(\Psi_0, \varphi_0)}(t, \varepsilon), f^2_{(\Psi_0, \varphi_0)}(t, \varepsilon)).$$

Working backward through the changes of coordinates that transformed (2.9) into (6.1) (see Appendix A for details), the linearly stable $2\pi\ell$-periodic solution (6.4) of (6.1) corresponds to a $2\pi\ell$-periodic solution of (2.9) which is such that

$$\Psi(t, \varepsilon) = f^1_{(\Psi_0, \varphi_0)}(t, \varepsilon) + R_{f^2_{(\Psi_0, \varphi_0)}(t, \varepsilon)} R_{kt/\ell} R_{\int_0^t h_2(s)\, ds}\, \mathcal{S}(t), \tag{6.5}$$

where $\mathcal{S}(t)$ is 2π-periodic (see Lemma A.2 and (A.3)). The term

$$R_{f^2_{(\Psi_0,\varphi_0)}(t,\varepsilon)} R_{kt/\ell} R_{\int_0^t h_2(s)\,ds}\,\mathcal{S}(t)$$

represents a compound motion of a 2π-periodic term $R_{\int_0^t h_2(s)\,ds}\,\mathcal{S}(t)$, a $2\pi\ell/k$-periodic term $R_{kt/\ell}$, and a $2\pi\ell$-periodic term $R_{f^2_{(\Psi_0,\varphi_0)}(t,\varepsilon)}$. Thus, this $2\pi\ell$-periodic solution corresponds to a two-frequency solution for (2.9), where the two frequencies are in ratio k/ℓ. If such a solution represents the dynamics of a spiral wave solution to (2.4) via the center manifold reduction (2.9), then the meander path of the spiral tip is closed and is composed of two frequencies which are in ratio k/ℓ. Moreover, because of the linear stability of this solution, it is stable to small perturbations in (2.4). This means that contrary to the fully Euclidean case, lattice symmetry-breaking may lead to phase-locking of meandering spiral waves.

In Figure 9, we illustrate meander paths for two simulations of (1.4) with different parameters, and with transients removed. We observe a phase-locked three-petal meandering path. The inhomogeneity functions g_1 and g_2 in (1.5) have the following coefficients for both simulations:

$$\varepsilon = 0.01,\ A_1 = -0.1997,\ A_2 = 0.2997,\ B_1 = 0.001,\ B_2 = -0.001,\ C_1 = -1,\ C_2 = 1.5. \tag{6.6}$$

6.1 Symmetry properties of (6.3).

The following is a direct consequence of the symmetry properties (2.10) for the functions G_1 and G_2 in (6.1) (which were proven in Proposition 3.2) and the definitions (6.2).

Proposition 6.2 *The averaged differential equations (6.3) are such that*

$$\mathcal{G}_1(-J\Psi, \varphi + \pi/2) = -J\mathcal{G}_1(\Psi,\varphi) \quad \text{and} \quad \mathcal{G}_2(-J\Psi, \varphi+\pi/2) = \mathcal{G}_2(\Psi,\varphi)$$

Proof This is a straightforward computation. ∎

It follows from Proposition 6.2 and Theorem 6.1 that if (Ψ_0, φ_0) is an equilibrium for (6.3), then there are conjugate equilibria $(-J^n\Psi_0, \varphi_0 + n\pi/2)$, $n = 0, 1, 2, 3$. Consequently, the $2\pi\ell$-periodic solutions (6.4) of (6.1) also come in conjugate families, and it follows from a straightforward computation that these possess the symmetry properties

$$\begin{aligned} f^1_{(-J\Psi_0,\varphi_0+\pi/2)}(\theta,\varepsilon) &= -Jf^1_{(\Psi_0,\varphi_0)}(\theta,\varepsilon), \\ f^2_{(-J\Psi_0,\varphi_0+\pi/2)}(\theta,\varepsilon) &= f^2_{(\Psi_0,\varphi_0)}(\theta,\varepsilon) + \pi/2. \end{aligned} \tag{6.7}$$

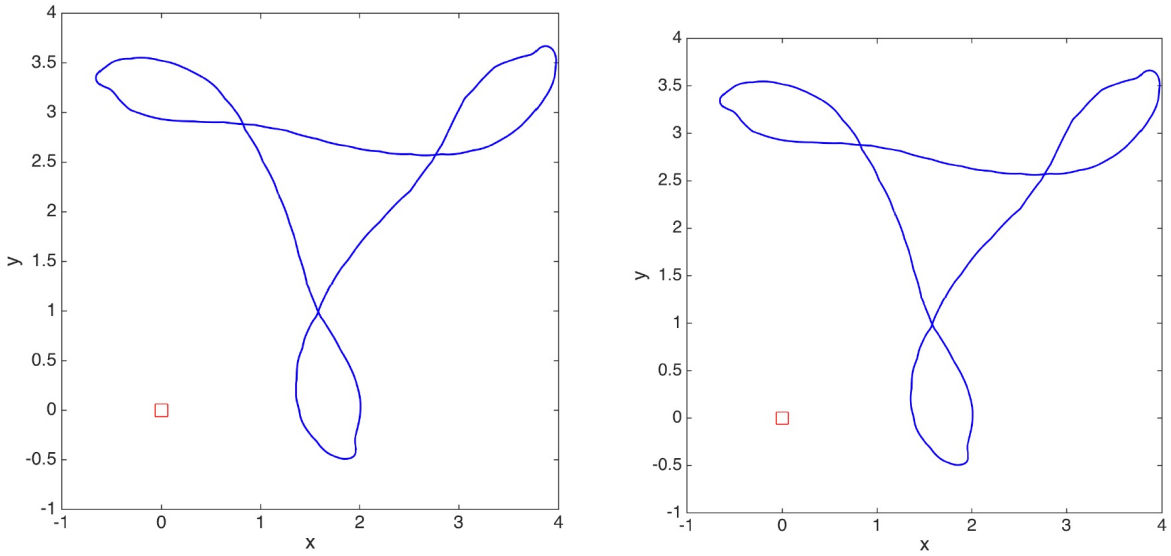

Figure 9: Meander paths of spiral waves in numerical simulations of (1.4) with inhomogeneity coefficients given by (6.6). The transients have been removed, and what is represented here is the final (steady) epicyclic meandering regime. The kinetic parameters are $\beta = 0.8$ and $\gamma = 0.5$ for both, and $\tau = 0.1018$ (left) and $\tau = 0.10195$ (right). The two-frequency three-petal motion thus appears to be phase-locked, as predicted by Theorem 6.1. The red square at $(0, 0)$ indicates a lattice point.

Now, depending on the denominator ℓ for $\omega = k/\ell$, the functions $\mathcal{G}_1$ and $\mathcal{G}_2$ may possess additional symmetries.

Proposition 6.3 *If ℓ is an integer multiple of 4, then*

$$\mathcal{G}_1(J\Psi,\varphi) = J\mathcal{G}_1(\Psi,\varphi) \quad \text{and} \quad \mathcal{G}_2(J\Psi,\varphi) = \mathcal{G}_2(\Psi,\varphi). \tag{6.8}$$

If ℓ is an integer multiple of 2, then

$$\mathcal{G}_1(-\Psi,\varphi) = -\mathcal{G}_1(\Psi,\varphi) \quad \text{and} \quad \mathcal{G}_2(-\Psi,\varphi) = \mathcal{G}_2(\Psi,\varphi). \tag{6.9}$$

Proof We will prove (6.8). The proof of (6.9) is similar, so we will omit it. Let n_1 and n_2 be integers such that

$$4\ell n_1 + 4kn_2 = \ell.$$

Such integers n_1 and n_2 exist since $\gcd(4\ell, 4k) = 4$, and ℓ is a multiple of 4. It follows that

$$\begin{aligned}
\mathcal{G}_1(J\Psi,\varphi) &= \frac{1}{2\pi\ell}\int_0^{2\pi\ell} R_\varphi R_{k\theta/\ell} G_1(J\Psi, \varphi + k\theta/\ell, \theta, 0)\, d\theta \\
&= \frac{1}{2\pi\ell}\int_0^{2\pi\ell} R_\varphi R_{k\theta/\ell} G_1(J\Psi, \varphi + (-2n_1+1/2)\pi + k\theta/\ell - \pi/2, \theta, 0)\, d\theta \\
&= \frac{1}{2\pi\ell}\int_0^{2\pi\ell} R_\varphi R_{k\theta/\ell} G_1(\Psi, \varphi + (-2n_1+1/2)\pi + k\theta/\ell, \theta, 0)\, d\theta \\
&= \frac{1}{2\pi\ell}\int_0^{2\pi\ell} R_\varphi R_{k\theta/\ell} G_1\left(\Psi, \varphi + \frac{k}{\ell}\left(\theta + \frac{\ell}{2k}(-4n_1+1)\pi\right), \theta, 0\right)\, d\theta \\
&= \frac{1}{2\pi\ell}\int_{\frac{\ell}{2k}(-4n_1+1)\pi}^{2\pi\ell+\frac{\ell}{2k}(-4n_1+1)\pi} R_\varphi R_{k\theta/\ell} R_{2n_1\pi} R_{-\pi/2} G_1(\Psi, \varphi + k\theta/\ell, \theta + 2\pi n_2, 0)\, d\theta \\
&= J\left(\frac{1}{2\pi\ell}\int_{2\pi n_2}^{2\pi\ell+2\pi n_2} R_\varphi R_{k\theta/\ell} G_1(\Psi, \varphi + k\theta/\ell, \theta, 0)\, d\theta\right) \\
&= J\left(\frac{1}{2\pi\ell}\int_0^{2\pi\ell} R_\varphi R_{k\theta/\ell} G_1(\Psi, \varphi + k\theta/\ell, \theta, 0)\, d\theta\right) = J\mathcal{G}_1(\Psi,\varphi).
\end{aligned}$$

A similar computation using the second equation in (6.2) reveals $\mathcal{G}_2(J\Psi,\varphi) = \mathcal{G}_2(\Psi,\varphi)$. ∎

These additional symmetry properties have the following consequence.

Corollary 6.4 *If $\omega = k/\ell$ ($\gcd(k,\ell) = 1$) is such that ℓ is even, then $\mathcal{G}_1$ in (6.3) is such that*

$$\mathcal{G}_1(0,\varphi) = 0 \quad \forall \varphi \in \mathbf{S}^1.$$

Therefore, the roots of the $\pi/2$ periodic function $\mathcal{G}_2(0,\varphi)$ correspond to equilibria of (6.3). If φ_0 is such that $\mathcal{G}_2(0,\varphi_0)=0$, and the equilibrium point $(0,\varphi_0)$ for (6.3) is hyperbolic, then the symmetry properties in (6.7) reduce to

$$\begin{aligned} f^1_{(0,\varphi_0+\pi/2)}(\theta,\varepsilon) &= -Jf^1_{(0,\varphi_0)}(\theta,\varepsilon), \\ f^2_{(0,\varphi_0+\pi/2)}(\theta,\varepsilon) &= f^2_{(0,\varphi_0)}(\theta,\varepsilon)+\pi/2. \end{aligned} \tag{6.10}$$

Proof This is a straightforward computation, using (6.8), (6.9), and the fact that J and $J^2=-I$ are rotation matrices which leave only the origin invariant. ∎

Proposition 6.5 *Let $\omega=k/\ell$ ($\gcd(k,\ell)=1$) be such that ℓ is even, and let $(0,\varphi_0)$ be a hyperbolic equilibrium point for (6.3). Then the $2\pi\ell$-periodic solution (6.4) of (6.1) has the spatiotemporal symmetry*

$$f^1_{(0,\varphi_0)}(\theta+\pi\ell,\varepsilon) = -f^1_{(0,\varphi_0)}(\theta,\varepsilon)$$

$$f^2_{(0,\varphi_0)}(\theta+\pi\ell,\varepsilon) = f^2_{(0,\varphi_0)}(\theta,\varepsilon).$$

If ℓ is an integer multiple of 4, we have the additional spatiotemporal symmetry

$$f^1_{(0,\varphi_0)}(\theta+\pi\ell/2,\varepsilon) = (-J)^k f^1_{(0,\varphi_0)}(\theta,\varepsilon)$$

$$f^2_{(0,\varphi_0)}(\theta+\pi\ell/2,\varepsilon) = f^2_{(0,\varphi_0)}(\theta,\varepsilon).$$

Proof Again, we will only prove the case where ℓ is an integer multiple of 4, the other case being similar. We note that the change of variables $\theta=\tilde\theta+\pi\ell/2$, $\tilde\varphi=\varphi+k\pi/2$ leaves (6.1) invariant. From this, it immediately follows that

$$f^1_{(0,\varphi_0)}(\theta,\varepsilon) = f^1_{(0,\tilde\varphi_0)}(\tilde\theta,\varepsilon), \quad f^2_{(0,\varphi_0)}(\theta,\varepsilon)+k\pi/2 = f^2_{(0,\tilde\varphi_0)}(\tilde\theta,\varepsilon),$$

or, equivalently,

$$f^1_{(0,\varphi_0)}(\theta+\pi\ell/2,\varepsilon) = f^1_{(0,\varphi_0+k\pi/2)}(\theta,\varepsilon), \quad f^2_{(0,\varphi_0)}(\theta+\pi\ell/2,\varepsilon)+k\pi/2 = f^2_{(0,\varphi_0+k\pi/2)}(\theta,\varepsilon). \tag{6.11}$$

But it follows from (6.10) that

$$\begin{aligned} f^1_{(0,\varphi_0+k\pi/2)}(\theta,\varepsilon) &= (-J)^k f^1_{(0,\varphi_0)}(\theta,\varepsilon) \\ f^2_{(0,\varphi_0+k\pi/2)}(\theta,\varepsilon) &= f^2_{(0,\varphi_0)}(\theta,\varepsilon)+k\pi/2. \end{aligned} \tag{6.12}$$

The conclusion follows from combining (6.11) with (6.12). ∎

Interpretation. For spiral waves, lattice symmetry-breaking can lead to phase-locked meandering spiral waves with even numbered "petals" which are anchored at a lattice point, and have spatiotemporal symmetry characterized as follows: rotating the meander path about the lattice point by an angle of π (or $\pi/2$ if the number of petals is a multiple of 4) is the same as advancing in time along the meander path by half (or a quarter) of the period. It follows that the meander paths as a whole are invariant under rotations by π (or $\pi/2$ if the number of petals is a multiple of 4).

In Figure 10, we illustrate meander paths for two simulations of (1.4) with different parameters and inhomogeneity functions. We observe in one case a phase-locked six-petal meandering path, and in another case a phase-locked four-petal meandering path. The rotational symmetries of these meander paths are consistent with the above remarks. The inhomogeneity functions g_1 and g_2 in (1.5) are

$$\varepsilon = 0.01,\ A_1 = 1.4,\ A_2 = 0.92,\ B_1 = 5,\ B_2 = 1,\ C_1 = -1,\ C_2 = 3 \tag{6.13}$$

for the six-petal path, and

$$\varepsilon = 0.01,\ A_1 = -1.75,\ A_2 = -0.35,\ B_1 = -6.25,\ B_2 = 1.25,\ C_1 = 1.25,\ C_2 = -3.75 \tag{6.14}$$

for the four-petal path.

6.2 Phase-locking windows and bifurcations.

As we have seen above, linearly stable equilibrium points of (6.3) correspond to linearly stable phase-locked commensurate frequency meandering solutions of (2.9). We are now interested in understanding how these solutions behave under variation of ω and ε.

In (3.2), we introduce an additional detuning parameter ζ and write $\omega = k/\ell + \varepsilon\zeta$ (with $\gcd(k,\ell) = 1$). By following the same procedure that we alluded to at the beginning of this section (see Theorem 6.1), we obtain a parametrized system of averaged equations analogous to (6.3):

$$\begin{aligned} \dot{\Psi} &= \varepsilon \mathscr{G}_1(\Psi, \varphi, \zeta) \\ \dot{\varphi} &= \varepsilon \mathscr{G}_2(\Psi, \varphi, \zeta). \end{aligned} \tag{6.15}$$

where the functions $\mathscr{G}_{1,2}$ possess the same symmetry properties as the functions $\mathcal{G}_{1,2}$ (respectively), and $\mathscr{G}_{1,2}(\Psi, \varphi, 0) = \mathcal{G}_{1,2}(\Psi, \varphi)$.

Therefore, if $(\omega, \varepsilon) = (k/\ell, \varepsilon_0)$ (with $\varepsilon_0 > 0$, $\gcd(k,\ell) = 1$) is such that (6.3) possesses such a linearly stable equilibrium point (Ψ_0, φ_0), then by using the implicit function theorem,

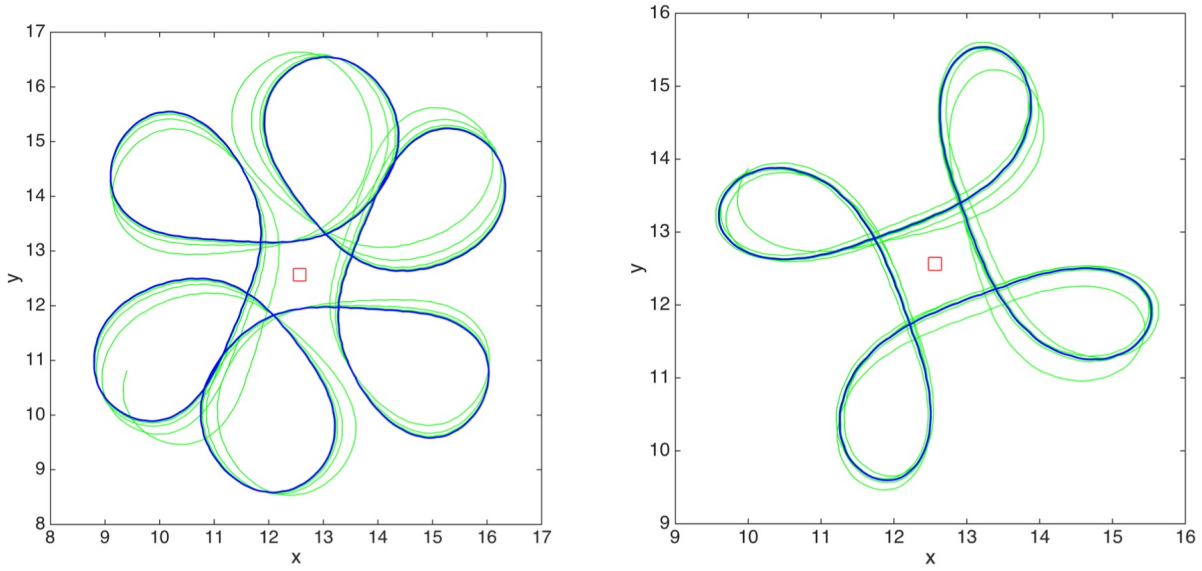

Figure 10: Meander paths of spiral waves in numerical simulations of (1.4) with inhomogeneity coefficients given by (6.13) (left) and by (6.14) (right). The transients are in green, and the final phase-locked meander path is in blue. The kinetic parameters are $(\beta, \gamma, \tau) = (0.87, 0.49, 0.22)$ (left) and $(\beta, \gamma, \tau) = (0.8, 0.65, 0.17)$ (right). The red square at $(4\pi, 4\pi)$ indicates a lattice point.

there is a neighborhood of the point $(0, \varepsilon_0)$ in (ζ, ε)-space where (6.15) possesses a linearly stable equilibrium point $(\Psi(\zeta,\varepsilon), \varphi(\zeta,\varepsilon))$ close to (Ψ_0, φ_0). From this argument, it follows that the ℓ-petal phase-locked meandering solution (6.5) of (2.9) which corresponds to (Ψ_0, φ_0) persists in a neighborhood of $(k/\ell, \varepsilon_0)$ in the (ω, ε) parameter space of (2.9) We call such a neighborhood a *phase-locking window* for (2.9). The boundary of such a phase-locking window thus corresponds to bifurcation of the equilibrium point $(\Psi(\zeta,\varepsilon), \varphi(\zeta,\varepsilon))$ of (6.15). Since the phase space of (6.15) is three-dimensional, then we could potentially observe higher-codimension bifurcations (e.g., mode interactions) in (6.15), and a thorough analysis will likely require the theoretical tools of [23] and [44]. We will not pursue this issue further in this paper. Instead, we will briefly address saddle-node and Hopf bifurcations.

6.2.1 Saddle-node bifurcation.

Phase-locked meander paths may lose stability via a saddle-node bifurcation of equilibria in (6.15). This phenomenon is very similar to the case where phase-locking is lost after exiting an Arnol'd tongue [4] in the theory of forced oscillators, so we will not pursue it in more detail here. In Figure 11, we see such a saddle-node bifurcation in (1.4) with inhomogeneity coefficients (1.5) given by (6.18).

6.2.2 Hopf bifurcation.

Here, we present what we believe to be a previously undocumented state for spiral waves. Suppose that for $\varepsilon = \varepsilon_0 > 0$ and $\zeta = \zeta_0$, the point (Ψ_0, φ_0) is an equilibrium point of (6.15), and that the linearization of (6.15) at $(\Psi_0, \varphi_0, \zeta_0)$ has a pair of complex conjugate eigenvalues on the imaginary axis and the other eigenvalue with negative real part. Then generically, as ζ varies near ζ_0, there will be a Hopf bifurcation, which will generate a limit cycle with amplitude of the order $O(\sqrt{|\zeta - \zeta_0|})$ (see, for example, [18, Theorem 3.4.2]). The criticality (i.e., super- or subcritical), as well as the stability of the bifurcating limit cycle, depends on the sign of the Lyapunov coefficient, which is obtained via Taylor coefficients of the vector field (6.15) at the point (Ψ_0, φ_0) (see, for example, formula (3.4.29) of [18]).

Heuristically, as a leading-order approximation, we write this limit cycle as

$$\Psi(t) = \Psi_0 + \sqrt{|\zeta - \zeta_0|}\,\mathscr{A}(t), \quad \varphi(t) = \varphi_0 + \sqrt{|\zeta - \zeta_0|}\,\mathscr{B}(t)$$

where $\mathscr{A}$ and $\mathscr{B}$ are $\mathscr{T}$-periodic, which leads to a leading-order approximation for the corresponding solution of (2.9),

$$\Psi_{\text{HB}}(t) = R_{\sqrt{|\zeta-\zeta_0|}\,\mathscr{B}(t)}\Psi(t), \tag{6.16}$$

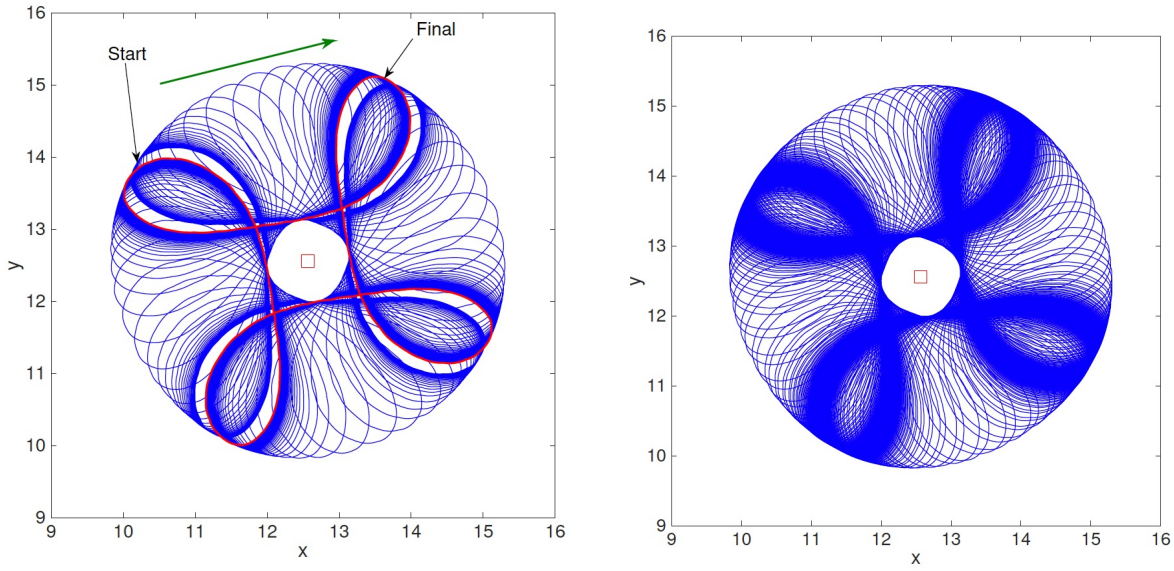

Figure 11: Saddle-node bifurcation of four-petal phase-locked meander paths in (1.4) with inhomogeneity coefficients (6.18). For both simulations, we have $\beta = 0.8$ and $\gamma = 0.65$. In the left figure ($\tau = 0.15818$), the meandering starts near an unstable four-petal flower (presumably located in the white gap), flows in the direction of the green arrow, and eventually settles onto the stable four-petal meandering state in red. In the right figure ($\tau = 0.15816$), the unstable and stable four-petal flowers have coalesced and disappeared in a saddle-node bifurcation, and the meandering is now unlocked (although we can still observe the slow transient passing through the remnants of the bifurcated states).

where $\Psi(t)$ is the ℓ-petal phase-locked path given by (6.5). In general, we expect that the period $\mathscr{T}$ will be incommensurate with $2\pi\ell$, and the resulting meander path (6.16) can best be described as a "fattened" ℓ-petal flower, with thickness $O(\sqrt{|\zeta-\zeta_0|})$: this fattening results from the small-amplitude time-periodic rotation $R_{\sqrt{|\zeta-\zeta_0|}\mathscr{B}(t)}$ of the overall ℓ-petal meander path (6.5) that is losing stability at the bifurcation. In the vocabulary of bifurcation theory, (6.16) represents a Naimark-Sacker bifurcation from the $2\pi\ell$-periodic phase-locked solution (6.5).

In Figure 12, we illustrate such a fattened three-petal flower in a simulation of (1.4) with inhomogeneity coefficients (1.5) given by

$$\varepsilon = 0.01,\ A_1 = -0.2,\ A_2 = 0.3,\ B_1 = 0,\ B_2 = 0,\ C_1 = -1,\ C_2 = 1.5. \tag{6.17}$$

In Figure 13, we illustrate how the image in Figure 12 originates in a Hopf bifurcation from varying the parameter τ in (1.4). Figure 14 illustrates a Hopf bifurcation from an anchored four-petal flower for system (1.4) with inhomogeneity data

$$\varepsilon = 0.01,\ A_1 = -0.082,\ A_2 = -0.014,\ B_1 = -0.1,\ B_2 = 0.05,\ C_1 = -0.25,\ C_2 = -0.15 \tag{6.18}$$

in (1.5).

7 Stable linear meandering waves in (3.3).

When $\varepsilon = 0$ in (3.3), its solutions can be expressed as

$$\varphi(t) = \varphi(0),\ \theta(t) = t + \theta(0),\ \Psi(t) = R_{\varphi(0)}Vt + \Psi(0). \tag{7.1}$$

Working backward through the changes of coordinates which transformed (2.9) into (3.3), this corresponds to linearly meandering traveling waves, such as that illustrated with the red meander path in Figure 5. In the context of full $\mathbf{SE}(2)$ symmetry (i.e., $\varepsilon = 0$), this phenomenon is not structurally stable, since arbitrarily small changes to the value of ω in (2.9) lead to a meander pattern which has (large radius) circular shape (green and blue meander paths in Figure 5).

In what follows, it will be helpful to interpret (7.1) in the following manner. Consider the hypersurface $\varphi = \text{constant} = \varphi(0)$ in $\mathbb{T}^4$. This hypersurface is diffeomorphic to a three-torus (parametrized by $\psi_{1,2}$ and θ). Equation (7.1) describes a linear flow on this three-torus, with frequencies given by the two components of $R_{\varphi(0)}V$ and 1. If these frequencies are rationally independent, then the solution curves for this linear flow are dense on the three-torus. We are interested in the persistence of such densely filled invariant three-tori when ε becomes nonzero.

Our main result in this section is the following theorem.

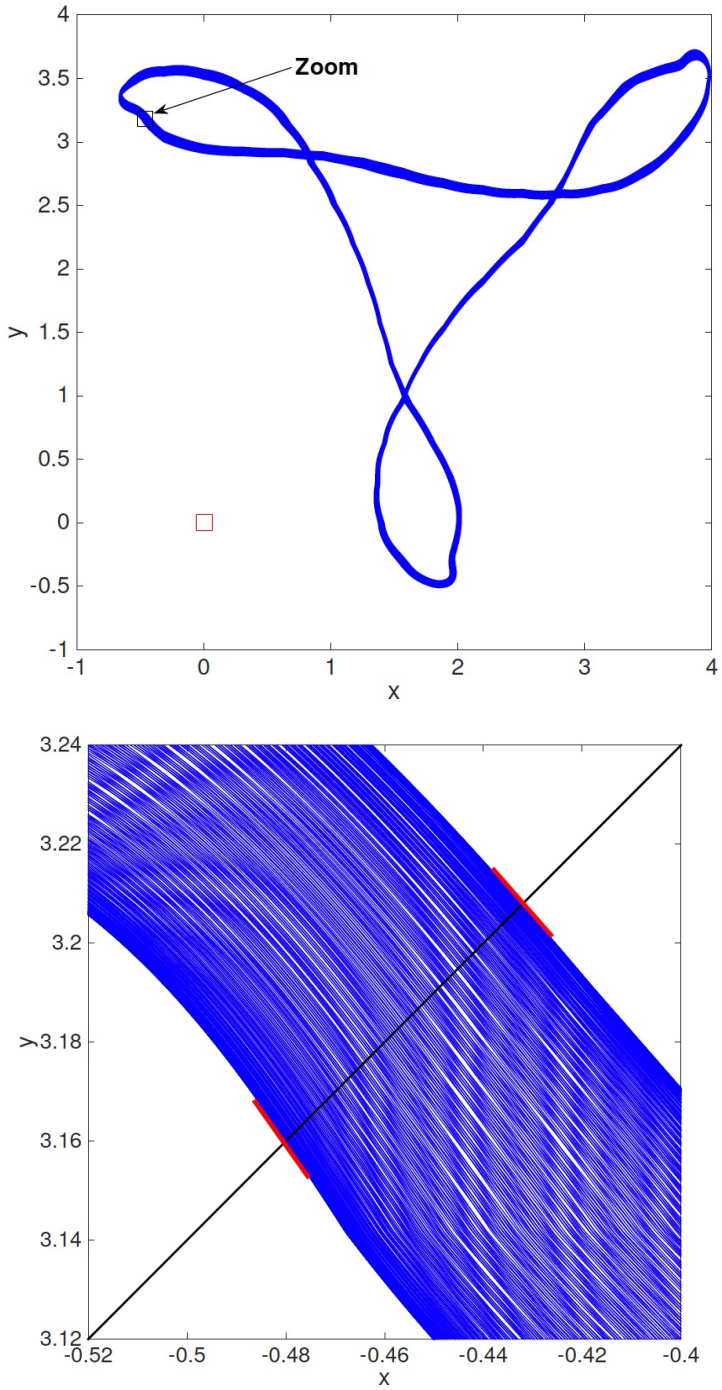

Figure 12: Fattened three-petal meander path observed in a simulation of (1.4) with inhomogeneity (6.17) and kinetic parameters $\tau = 0.1014$, $\beta = 0.8$, $\gamma = 0.5$ (transients removed). The bottom figure is a close-up view of the inset box in the top figure. As an admittedly arbitrary measure of the thickness, we choose the length between the two little red lines of the black segment (line connecting the point $(-0.52, 3.12)$ to the point $(-0.40, 3.24)$). In this case, it measures 0.06760. In Figure 13 below, we illustrate how this meander path originates from a Hopf bifurcation from a phase-locked three-petal meander path.

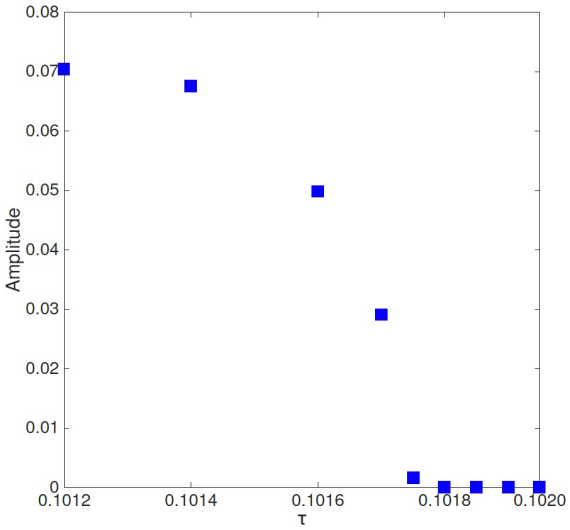

Figure 13: Amplitude (measured as described in the caption of Figure 12) of fattened three-petal meander path as a function of τ for nine simulations of (1.4). The inhomogeneity data and values for β and γ are the same as in Figure 12, and τ is varied from 0.1012 to 0.1020. We observe the characteristic shape of a Hopf bifurcation diagram.

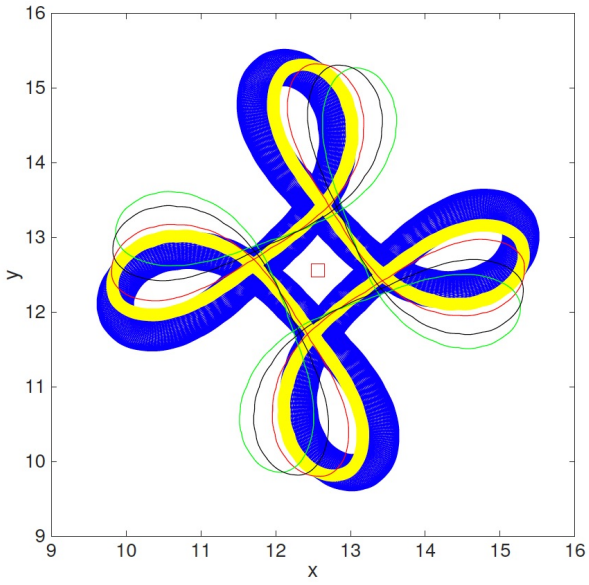

Figure 14: Hopf bifurcation of a phase-locked symmetric four-petal meander path in (1.4) with inhomogeneity data (6.18). For each of the five simulations, we have $\beta = 0.8$ and $\gamma = 0.65$. The phase-locked paths (prior to bifurcation) are green ($\tau = 0.1586$), black ($\tau = 0.1590$), and red ($\tau = 0.1596$). The bifurcated (fattened) paths are yellow ($\tau = 0.1600$) and blue ($\tau = 0.1604$).

Theorem 7.1 *Consider the system (3.3), and define the function*

$$\mathcal{Z}(\varphi) = \langle H_2(\cdot, \varphi, \cdot, 0)\rangle \equiv \frac{1}{(2\pi)^3}\int_{\mathbb{T}^3} H_2(\Psi, \varphi, \theta, 0)d\Psi d\theta$$

Let φ_0 be such that $\mathcal{Z}(\varphi_0) = 0$, and let $\alpha = \mathcal{Z}'(\varphi_0) \neq 0$. Define the real numbers ω_1 and ω_2 as the components of the two-dimensional vector $R_{\varphi_0}V$, and suppose that $\mathbf{\Omega} = (\omega_1, \omega_2, 1)$ satisfies the Diophantine condition of Definition 4.1. Then for all $\varepsilon > 0$ sufficiently small, (3.3) has an invariant three-torus

$$\varphi = \mathscr{L}(\Psi, \theta, \varepsilon), \quad \mathscr{L}(\Psi, \theta, \varepsilon) \to \varphi_0, \ \text{ as } \ \varepsilon \to 0.$$

This invariant three-torus is locally asymptotically stable (resp., unstable) if $\alpha < 0$ (resp., $\alpha > 0$).

Proof The proof closely follows that of Theorem 5.1 of [12], with minor changes accounting for the additional angular variable θ. Therefore, we only give a sketch of the main points. First, we make the change of variables

$$\varphi \to \varphi_0 + \sqrt{\varepsilon}\,\varphi$$

and perform a Taylor expansion of (3.3) to get

$$\begin{aligned}
\dot{\Psi} &= R_{\varphi_0}V + \sqrt{\varepsilon}R'_{\varphi_0}V\varphi + \varepsilon(R_{\varphi_0}H_1(\Psi, \varphi_0, \theta, 0) + \tfrac{1}{2}R''_{\varphi_0}V\varphi^2) + \varepsilon^{\frac{3}{2}}Q_1(\Psi, \varphi, \theta, \varepsilon)\\
\dot{\varphi} &= \sqrt{\varepsilon}H_2(\Psi, \varphi_0, \theta, 0) + \varepsilon H_{2,\varphi}(\Psi, \varphi_0, \theta, 0)\varphi + \varepsilon^{\frac{3}{2}}(\tfrac{1}{2}H_{2,\varphi\varphi}(\Psi, \varphi_0, \theta, 0)\varphi^2 + H_{2,\varepsilon}(\Psi, \varphi_0, \theta, 0))\\
&\quad +\varepsilon^2 S_1(\Psi, \varphi, \theta, \varepsilon)\\
\dot{\theta} &= 1,
\end{aligned} \tag{7.2}$$

for smooth functions Q_1 and S_1. Since the function $H_2(\Psi, \varphi_0, \theta, 0)$ has zero mean value, i.e. $\langle H(\cdot, \varphi_0, \cdot, 0)\rangle = Z(\varphi_0) = 0$, then it follows from Proposition 4.2 that there exists a smooth function $\mathcal{Y}_1(\Psi, \theta)$ such that

$$D_\Psi \mathcal{Y}_1(\Psi, \theta)R_{\varphi_0}V + D_\theta \mathcal{Y}_1(\Psi, \theta) = H_2(\Psi, \varphi_0, \theta, 0).$$

We now perform, in succession, the following changes of variables

- $\varphi \to \varphi + \sqrt{\varepsilon}\mathcal{Y}_1(\Psi, \theta)$,
- $\varphi \to \sqrt{\varepsilon}\varphi$,

- $\varphi \to \varphi + \varepsilon(\mathcal{Y}_2(\Psi,\theta) + \varphi\mathcal{Y}_3(\Psi,\theta))$,
- $\Psi \to \Psi + \varepsilon\mathcal{Y}_4(\Psi,\theta)$,

where $\mathcal{Y}_{2,3,4}$ are suitably chosen (via Proposition 4.2) to annihilate certain terms in the ODE. Equation (7.2) then becomes

$$\begin{aligned} \dot{\Psi} &= R_{\varphi_0}V + \varepsilon(R'_{\varphi_0}V\varphi + \kappa) + O(\varepsilon^{\frac{3}{2}}) \\ \dot{\varphi} &= \varepsilon(\alpha\varphi + c) + O(\varepsilon^{\frac{3}{2}}) \\ \dot{\theta} &= 1, \end{aligned} \tag{7.3}$$

where α is as in the statement of the theorem, and

$$\kappa = \langle R_{\varphi_0}H_1(\cdot,\varphi_0,\cdot,0)\rangle,$$

$$c = \langle H_{2,\varepsilon}(\cdot,\varphi_0,\cdot,0) + H_{2,\varphi}(\cdot,\varphi_0,\cdot,0)\mathcal{Y}_1(\cdot,\cdot) - D_\Psi\mathcal{Y}_1(\cdot,\cdot)(R_{\varphi_0}H_1(\cdot,\varphi_0,\cdot,0) + R'_{\varphi_0}V\mathcal{Y}_1(\cdot,\cdot))\rangle.$$

A simple translation of the variable φ in (7.3) renders the equation in the proper form to apply Theorem 3.1 and get the conclusion. ∎

Interpretation. In fully **SE**(2) symmetric dynamical systems (such as (1.4) with $\varepsilon = 0$), modulated traveling waves are not structurally stable. This is illustrated in Figure 1 of [8], where modulated traveling waves occur only on a line (dashed curve) in the $\beta - \tau$ parameter space of (1.4) with $\varepsilon = 0$ and $\gamma = 0.5$. Ashwin, Melbourne, and Nicol [5] explain this as a codimension 1 drift bifurcation on group orbits of solutions to **SE**(2)-equivariant dynamical systems.

Theorem 7.1 implies that under certain conditions, it is possible for a lattice symmetry-breaking perturbation in (1.4) to render modulated traveling waves structurally stable. Figure 15 appears to illustrate this phenomenon. In this figure, we show the meander paths for three numerical simulations of (1.4) using the same kinetic parameters as those of Figure 5 (homogeneous case), but with inhomogeneity data (1.5) given by

$$\varepsilon = 0.01,\ A_1 = -0.6,\ A_2 = -0.4,\ B_1 = -0.00005,\ B_2 = 0.00007,\ C_1 = -3,\ C_2 = -2 \tag{7.4}$$

and same initial condition for all three simulations. This figure should be compared and contrasted to Figure 5.

8 Discussion.

Discrete regular (periodic) spatial structures are ubiquitous in nature. In electrophysiological tissue, these structures are arrays of excitable cells coupled together through gap

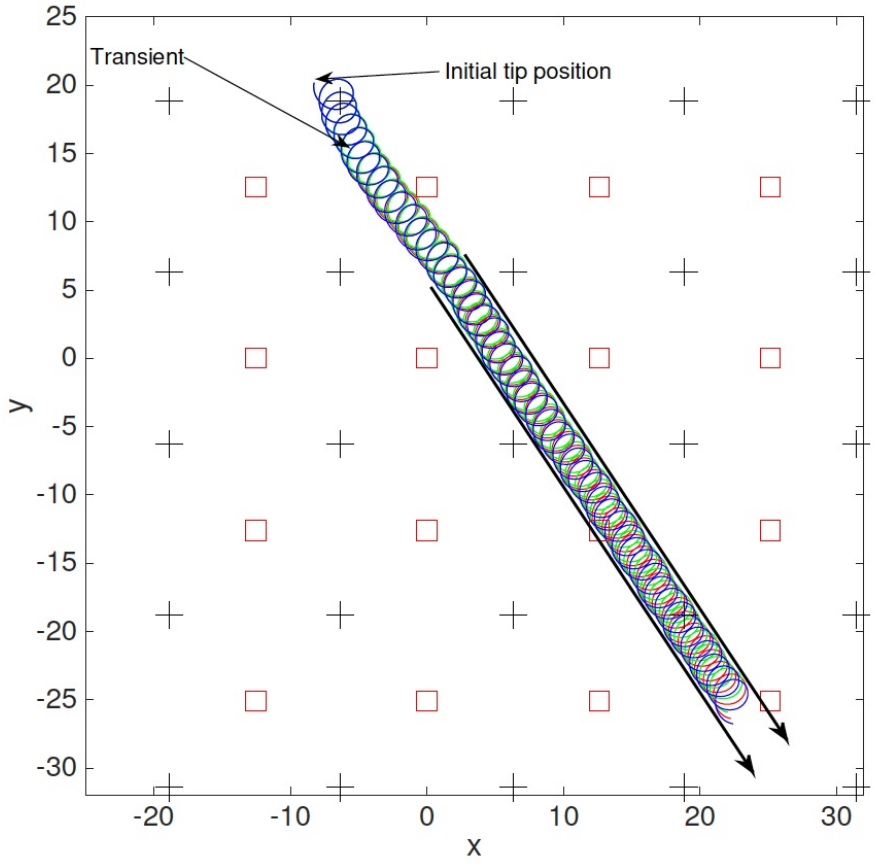

Figure 15: Superposition of meander paths for three simulations of (1.4) with inhomogeneity data given by (7.4) and the same initial condition in all three cases. These paths are consistent with a structurally stable modulated traveling wave, as predicted by Theorem 7.1. Parameter values are $\tau = 0.26$, $\gamma = 0.5$, and $\beta = 0.793$ (green), $\beta = 0.79275$ (blue), $\beta = 0.792875$ (red). The parallel black arrows on both sides of the meander paths have been added to the figure to guide the eye, and the red squares and black crosses represent the lattice and dual lattice points, respectively.

junctions. In many instances, treating these structures as a homogeneous continuum, and deriving PDEs based on this assumption (using homogenization techniques), is a reasonable low-order approximation and leads to many successful predictions about the system being modeled. However, if the solutions we are interested in studying display features that are of a size comparable in order to the cellular structure, then the continuum assumption may not be of sufficient complexity to capture the dynamical properties of these solutions. Furthermore, numerical simulations of spiral waves in homogeneous RDPDEs using coarse spatial discretization may introduce spurious dynamical properties, which are inconsistent with a homogeneous model. This paper is an attempt to characterize certain generic, qualitative phenomenological effects that a lattice structure may induce on meandering spiral waves in two-dimensional excitable media. As was the case in previous studies [10, 12, 24, 26], we have shown that a weak lattice perturbation has stabilizing (in physical space) effects on the meandering motion, alters the spatiotemporal symmetry properties of the meander path, and can lead to phase-locked solutions. We also presented what we believe to be a previously undocumented case for spiral wave meandering: the so-called "fattened" ℓ-petal flower which originates in a Hopf bifurcation from a phase-locked ℓ-petal epicyclic meandering wave.

As we mentioned in the introduction, one could make a compelling case that perhaps different geometries of lattices would be more appropriate in certain arrangements of excitable cells (e.g., hexagonal). However, the purpose of this paper was not to describe any one physical situation in particular but to gain an understanding of how spatially organized discrete structures may affect spiral wave dynamics. Certainly, one could repeat the analysis of this paper, replacing the square lattice by a hexagonal lattice. We expect that the number theoretical aspects of which meander paths get anchored at lattice points, as well as spatiotemporal symmetries would change, but we do not expect any fundamentally new qualitative results. One could also adopt a purely discrete approach − for example, studying spirals in lattice dynamical systems (LDS) [30]. But then one would lose the aspect that much of the observed spiral wave dynamics are driven by and originate in Euclidean symmetry. This is one of the advantages of our forced symmetry-breaking approach: we are in a sense studying systems that interpolate the fully Euclidean continuum RDPDE and completely discrete LDS. We thus expect that the results presented herein will be important in the largely unexplored study of meandering spiral waves in two-dimensional LDS.

We also note that the reduction of the infinite-dimensional problem (2.4) into the finite-dimensional center-bundle equations (2.9) requires a spectral gap condition in Hypothesis 2.2. While this hypothesis holds for a large variety of spirals (such as decaying amplitude spirals), there is also a large family of spirals for which this fails to hold, including Archimedean spirals. See [37] for a thorough discussion on these spectral issues. Even if the spiral does not decay (e.g., Archimedean spirals), the center bundle ODEs apparently still describe remarkably well many of the experimentally observed dynamics of the wave. Thus, the

study of Euclidean-equivariant ODEs on finite-dimensional noncompact manifolds, and their perturbations, is a central idea in the study of the dynamics and bifurcations of spiral waves, and it is the one we have adopted here.

As a final remark, we note that one of the strengths of our approach in this paper is also perhaps one of its weaknesses, depending on one's purpose. By adopting a model-independent approach as we have done here (i.e., computations and analysis driven mostly by symmetry considerations), we capture some robust generic features of the effects of lattice symmetry-breaking for a large class of mathematical models, without much consideration for the finer details of the models. The most important requirement is that we have a mathematical model where spiral waves are known to exist, and the model is weakly heterogeneous in space, with heterogeneities on a lattice. So in this sense, our results are potentially broad in applicability. However, one can imagine situations where it may be important, when studying a specific model (e.g., RDPDE such as (1.4)), to know the explicit link between the model parameters (e.g., τ, β, γ, ε, g_1, and g_2) and the quantities which arise in the center-bundle equations (2.9). As mentioned earlier in this paper in Remark 2.4(a), although such a link theoretically exists, it is in practice usually unfeasible to explicitly compute this link (see, however, [39]), unless one has explicit knowledge of the mathematical representation (e.g., algebraic formula) for the spiral wave.

Acknowledgments

This research is partly supported by the Natural Sciences and Engineering Research Council of Canada in the form of a Discovery Grant (VGL). One of the authors (PMK) thanks the Department of Mathematics and Statistics at the University of Ottawa for hosting his postdoctoral fellowship during which this paper was written.

Appendix

A Proofs of Propositions 3.2 and 3.3.

The proofs for both these propositions follow one another closely except for some subtle technical differences. We will first give the proof of Proposition 3.2 and then indicate the modifications which need to be made in order to prove Proposition 3.3.

The function $h_2(\theta)$ in (2.9) satisfies (2.6). We recall the definition of the rotation matrix R_ϕ in (2.2), and that $J = R_{-\pi/2}$. We note that $\frac{d}{d\phi}R_\phi = -JR_\phi$.

If we define

$$K(\theta) = R_{\int_0^\theta h_2(s)ds} h_1(\theta), \tag{A.1}$$

then it is easy to show that $K(\theta)$ is 2π-periodic in θ. We then have the following lemma.

Lemma A.1 *If ω is not an integer, then there exists a 2π-periodic function $M(\theta)$ such that*

$$\frac{d}{d\theta}M(\theta) - \omega J M(\theta) = K(\theta). \tag{A.2}$$

Proof Write $K(\theta)$ and $M(\theta)$ as Fourier series $K(\theta) = \sum_{k\in\mathbb{Z}} R_{k\theta}\hat{B}_k$, $M(\theta) = \sum_{k\in\mathbb{Z}} R_{k\theta}\hat{A}_k$, where the coefficients $\hat{A}_k$ and $\hat{B}_k$ are in $\mathbb{R}^2$. Then (A.2) is satisfied provided $\hat{A}_k$ and $\hat{B}_k$ satisfy the algebraic equation

$$-(k+\omega)J\hat{A}_k = \hat{B}_k \Longrightarrow \hat{A}_k = \frac{1}{k+\omega}J\hat{B}_k.$$

Uniform convergence of the series for M follows from the uniform convergence of the series for K. ∎

Lemma A.2 *Let $M(\theta)$ be as in Lemma A.1. Define $\mathcal{S}(\theta) = R_{-\int_0^\theta h_2(s)ds}M(\theta)$ and $\mathcal{Q}(\varphi,\theta) = R_\varphi\mathcal{S}(\theta)$. Then $\mathcal{Q}$ is 2π-periodic in both φ and θ, and satisfies the linear PDE*

$$(\omega + h_2(\theta))\frac{\partial\mathcal{Q}}{\partial\varphi} + \frac{\partial\mathcal{Q}}{\partial\theta} = R_\varphi h_1(\theta).$$

Proof The periodicity properties are obvious. Using the fact that M satisfies (A.2) and $(R_\phi)' = -JR_\phi$, we compute

$$\frac{\partial\mathcal{S}}{\partial\theta} = h_1(\theta) + (\omega + h_2(\theta))J\mathcal{S}(\theta),$$

from which it follows that

$$\frac{\partial\mathcal{Q}}{\partial\varphi} = -JR_\varphi\mathcal{S}(\theta) \quad \text{and} \quad \frac{\partial\mathcal{Q}}{\partial\theta} = R_\varphi[h_1(\theta) + (\omega + h_2(\theta))J\mathcal{S}(\theta)].$$

The conclusion now follows from a simple computation. ∎

Now, setting

$$\hat{\Psi} = \Psi - \mathcal{Q}(\varphi,\theta)(\text{modulo } \mathbb{T}^2), \tag{A.3}$$

and using the above lemmas, the system (2.9) becomes

$$\begin{aligned}\dot{\hat{\Psi}} &= \varepsilon R_\varphi \mathscr{M}_1(\hat{\Psi},\varphi,\theta,\varepsilon)\\ \dot{\varphi} &= \omega + h_2(\theta) + \varepsilon \mathscr{M}_2(\hat{\Psi},\varphi,\theta,\varepsilon)\\ \dot{\theta} &= 1,\end{aligned}$$

where

$$\mathscr{M}_1(\hat{\Psi},\varphi,\theta,\varepsilon) = F_1(\hat{\Psi}+\mathcal{Q}(\varphi,\theta),\varphi,\theta,\varepsilon) + J\mathcal{S}(\theta)F_2(\hat{\Psi}+\mathcal{Q}(\varphi,\theta),\varphi,\theta,\varepsilon)$$

and

$$\mathscr{M}_2(\hat{\Psi},\varphi,\theta,\varepsilon) = F_2(\hat{\Psi}+\mathcal{Q}(\varphi,\theta),\varphi,\theta,\varepsilon).$$

The functions $\mathscr{M}_{1,2}$ satisfy the symmetry properties (2.10) since the functions $F_{1,2}$ satisfy these properties, and

$$\mathcal{Q}(\varphi+\pi/2,\theta) = R_{\varphi+\pi/2}\mathcal{S}(\theta) = R_{\pi/2}R_\varphi\mathcal{S}(\theta) = -J\mathcal{Q}(\varphi,\theta).$$

Finally, setting $\hat{\varphi} = \varphi - \int_0^\theta h_2(s)ds$ (modulo $\mathbb{T}^1$) we obtain (3.2) (after dropping the hats), where

$$G_1(\hat{\Psi},\hat{\varphi},\theta,\varepsilon) = R_{\int_0^\theta h_2(s)ds}\mathscr{M}_1(\hat{\Psi},\hat{\varphi}+\int_0^\theta h_2(s)ds,\theta,\varepsilon),$$

$$G_2(\hat{\Psi},\hat{\varphi},\theta,\varepsilon) = \mathscr{M}_2(\hat{\Psi},\hat{\varphi}+\int_0^\theta h_2(s)ds,\theta,\varepsilon)$$

also satisfy the symmetry properties (2.10). This ends the proof of Proposition 3.2 ∎

To prove Proposition 3.3, we define $K(\theta)$ as in (A.1). Let $j \in \mathbb{Z}$ be such that $\omega = -j$. If the Fourier series for $K(\theta)$ is $K(\theta) = \sum_{k\in\mathbb{Z}} R_{k\theta}\hat{B}_k$, then define

$$\tilde{K}(\theta) = \sum_{k\in\mathbb{Z},k\neq j} R_{k\theta}\hat{B}_k$$

so that

$$K(\theta) = \tilde{K}(\theta) + R_{j\theta}\hat{B}_j.$$

We then have the following lemma.

Lemma A.3 *If $\omega = -j \in \mathbb{Z}$, then there exists a 2π-periodic function $\tilde{M}(\theta)$ such that*

$$\frac{d}{d\theta}\tilde{M}(\theta) - \omega J\tilde{M}(\theta) = \tilde{K}(\theta),$$

whose proof follows that of Lemma A.1, considering that the Fourier series for $\tilde{K}$ is such that the term for $k = j$ vanishes, so we can set $A_j = 0$ in the Fourier series for $\tilde{M}$.

Lemma A.2 is replaced by

Lemma A.4 *Let $\tilde{M}(\theta)$ be as in Lemma A.3. Define $\tilde{\mathcal{S}}(\theta) = R_{-\int_0^\theta h_2(s)ds}\tilde{M}(\theta)$ and $\tilde{\mathcal{Q}}(\varphi,\theta) = R_\varphi\tilde{\mathcal{S}}(\theta)$. Then $\tilde{\mathcal{Q}}$ is 2π-periodic in both φ and θ, and satisfies the linear partial differential equation*

$$(\omega + h_2(\theta))\frac{\partial\tilde{\mathcal{Q}}}{\partial\varphi} + \frac{\partial\tilde{\mathcal{Q}}}{\partial\theta} = R_\varphi[h_1(\theta) - R_{-\int_0^\theta h_2(s)ds}R_{j\theta}B_j]$$

Performing the change of variables $\hat{\Psi} = \Psi - \tilde{\mathcal{Q}}(\varphi,\theta)$ on (2.9) yields (upon dropping the hats)

$$\begin{aligned}\dot{\Psi} &= R_\varphi R_{j\theta-\int_0^\theta h_2(s)ds}B_j + \varepsilon R_\varphi\mathscr{N}_1(\Psi,\varphi,\theta,\varepsilon)\\ \dot{\varphi} &= \omega + h_2(\theta) + \varepsilon\mathscr{N}_2(\Psi,\varphi,\theta,\varepsilon)\\ \dot{\theta} &= 1,\end{aligned}$$

where

$$\mathscr{N}_1(\Psi,\varphi,\theta,\varepsilon) = F_1(\Psi + \tilde{\mathcal{Q}}(\varphi,\theta),\varphi,\theta,\varepsilon) + J\tilde{\mathcal{S}}(\theta)F_2(\Psi + \tilde{\mathcal{Q}}(\varphi,\theta),\varphi,\theta,\varepsilon)$$

and

$$\mathscr{N}_2(\Psi,\varphi,\theta,\varepsilon) = F_2(\Psi + \tilde{\mathcal{Q}}(\varphi,\theta),\varphi,\theta,\varepsilon).$$

The functions $\mathscr{N}_{1,2}$ satisfy the symmetry properties (2.10) since the functions $F_{1,2}$ satisfy these properties, and

$$\tilde{\mathcal{Q}}(\varphi+\pi/2,\theta) = R_{\varphi+\pi/2}\tilde{\mathcal{S}}(\theta) = R_{\pi/2}R_\varphi\tilde{\mathcal{S}}(\theta) = -J\tilde{\mathcal{Q}}(\varphi,\theta).$$

Finally, setting $\hat{\varphi} = \varphi - \int_0^\theta h_2(s)ds + j\theta$ in the above system and dropping the hats gives us (3.3), where $V \equiv \hat{B}_j$ and

$$H_1(\Psi,\varphi,\theta,\varepsilon) = R_{\int_0^\theta h_2(s)ds}R_{-j\theta}\mathscr{N}_1(\Psi,\varphi+\int_0^\theta h_2(s)ds - j\theta,\theta,\varepsilon)$$

$$H_2(\Psi,\varphi,\theta,\varepsilon) = \mathscr{N}_2(\Psi,\varphi+\int_0^\theta h_2(s)ds - j\theta,\theta,\varepsilon),$$

which satisfy the symmetry properties (2.10). This ends the proof of Proposition 3.3. ∎

References

[1] A. Adamatzky and O. Holland. Phenomenology of excitation in 2-D cellular automata and swarm systems. *Chaos, Solitons and Fractals*, **9** 1233 – 1265, 1998.

[2] K. Agladze, D. Jackson and T. Romeo. Periodicity of Cell Attachment Patterns during Escherichia coli Biofilm Development. *J. Bacteriology*, **185** 5632 – 5638, 2003.

[3] P. K. Anhelt, H. Kolb and R. Pflug. Identification of a subtype of cone photoreceptor, likely to be blue sensitive, in the human retina. *J. Comp. Neurol.*, **255** 18–34, 1987.

[4] V. I. Arnol'd. *Geometrical Methods in the Theory of Ordinary Differential Equations, 2nd Ed.* A Series of Comprehensive Studies in Mathematics **250**, Springer-Verlag, New-York, 1988.

[5] P. Ashwin, I. Melbourne and M. Nicol. Drift Bifurcations of Relative Equilibria and Transitions of Spiral Waves. *Nonlinearity*, **12** 741 – 755, 1999.

[6] D. Barkley. Linear stability analysis of rotating spiral waves in excitable media. *Phys. Rev. Lett.*, **68** 2090–2093, 1992.

[7] D. Barkley. Euclidean symmetry and the dynamics of rotating spiral waves. *Phys. Rev. Lett.*, **72** 165–167, 1994.

[8] D. Barkley and I. G. Kevrekidis. A dynamical systems approach to spiral wave dynamics. *Chaos*, **4** 453–460,1994.

[9] D. Barkley, M. Kness and L. S. Tuckerman. Spiral-wave dynamics in a simple model of excitable media: The transition from simple to compound rotation. *Phys. Rev. A*, **42** 2489–2492, 1990.

[10] P. Boily, V. G. LeBlanc, and E. Matsui. Spiral anchoring in media with multiple inhomogeneities: a dynamical system approach. *J. Nonlin. Sc.*, **17** 399 – 427, 2007.

[11] Y. Bourgault, M. Ethier, and V.G. LeBlanc. Simulation of Electrophysiological Waves with an Unstructured Finite Element Method. *ESAIM: Mathematical Modelling and Numerical Analysis*, **37**, 649 – 662, 2003.

[12] L. Charette, and V. G. LeBlanc. Lattice symmetry-breaking perturbations for spiral waves. *SIAM Journal of Applied Dynamical Systems*, **13** 1694–1715, 2014.

[13] J. M. Davidenko, A. V. Pertsov, R. Salomonsz, W. Baxter, J. Jalife. Stationary and drifting spiral waves of excitation in isolated cardiac tissue. *Nature*, **355** 349–351, 1992.

[14] A. Fasano and S. Marmi. *Analytical Mechanics.* Oxford University Press, New York, 2006.

[15] M. Golubitsky, V. G. LeBlanc and I. Melbourne. Meandering of the Spiral Tip: An Alternative Approach. *J. Nonlin. Sc.*, **7** 557 – 586, 1997.

[16] M. Golubitsky, V. G. LeBlanc and I. Melbourne. Hopf Bifurcation from Rotating Waves and Patterns in Physical Space. *J. Nonlin. Sc.*, **10** 69 – 101, 2000.

[17] M. Golubitsky and I. Stewart. *The Symmetry Perspective: From Equilibrium to Chaos in Phase Space and Physical Space.* Progress in Mathematics **200**, Birkhäuser Verlag, Berlin, 2000.

[18] J. Guckenheimer and P. J. Holmes. *Nonlinear Oscillations, Dynamical Systems and Bifurcations of Vector Fields.* Applied Math. Sci. **42**, Springer-Verlag, New York, 1983.

[19] J. K. Hale. *Ordinary Differential Equations, 2nd Ed.* Robert E. Krieger Publishing Company, Florida, 1980.

[20] D. Henry. *Geometric theory of semilinear parabolic equations.* Lecture Notes in Mathematics **804**, Springer-Verlag, New York, 1981.

[21] X. Huang, W. C. Troy, Q. Yang, H. Ma, C. R. Laing, S. J. Schiff, and J. Y. Yu. Spiral waves in disinhibited mammalian neocortex. *J. Neurosci.* **24**, 9897–9902, 2004.

[22] J. Keener and J. Sneyd. *Mathematical Physiology.* Interdisciplinary Applied Mathematics **8**, Springer-Verlag, New York, 1998.

[23] J. S. W. Lamb and I. Melbourne. Bifurcation from discrete rotating waves. *Arch. Rat. Mech. Anal.*, **149** 229–270, 1999.

[24] V. G. LeBlanc. Rotational symmetry-breaking for spiral waves. *Nonlinearity*, **15** 1179 – 1203, 2002.

[25] V. G. LeBlanc and B. J. Roth Meandering of spiral waves in anisotropic tissue. *Dynamics of Continuous, Discrete and Impulsive Systems, Series B*, **10**, 29 – 42, 2003.

[26] V. G. LeBlanc and C. Wulff. Translational symmetry-breaking for spiral waves. *J. Nonlin. Sc.*, **10** 569 – 601, 2000.

[27] G. Li, Q. Ouyang, V. Petrov and H. L. Swinney. Transition from simple rotating chemical spirals to meandering and traveling spirals. *Phys. Rev. Lett.*, **77** 2105–2108, 1996.

[28] L. Mesin. Dynamics of spiral waves in a cardiac electromechanical model with a local electrical inhomogeneity. *Chaos Solitons Fractals*, **45** 1220 – 1230, 2012.

[29] A. P. Muñuzuri, V. Pérez-Muñuzuri and V. Pérez-Villar. Attraction and Repulsion of Spiral Waves by Localized Inhomogeneities in Excitable Media. *Phys. Rev. E*, **58** R2689 – R2692, 1998.

[30] J. E. Paullet and G. B. Ermentrout. Stable rotating waves in two-dimensional discrete active media. *SIAM J. Appl. Math.*, **54** 1720–1744, 1994.

[31] M. C. Pereyra and L. A. Ward. *Harmonic Analysis from Fourier to wavelets.* Student Mathematical Library, IAS/Park City Mathematical Subseries **63**, AMS, Providence, 2012.

[32] A. V. Pertsov, J. M. Davidenko, R. Salomonsz, W. Baxter, J. Jalife Spiral waves of excitation underlie reentrant activity in isolated cardiac muscle. *Circ. Res.*, **72** 631–650, 1993.

[33] B. J. Roth. Frequency locking of meandering spiral waves in cardiac tissue. *Phys. Rev. E*, **57** R3735 – R3738, 1998.

[34] B. J. Roth. Meandering of spiral waves in anisotropic cardiac tissue. *Physica D*, **150** 127 – 136, 2001.

[35] B. Sandstede, A. Scheel, and C. Wulff. Dynamics of spiral waves on unbounded domains using center-manifold reductions. *J. Diff. Eq.*, **141** 122 – 149, 1997.

[36] B. Sandstede, A. Scheel, and C. Wulff. Bifurcation and Dynamics of Spiral Waves. *J. Nonlin. Sc.*, **9** 439 – 478, 1999.

[37] A. Scheel. Bifurcation to spiral waves in reaction-diffusion systems. *SIAM J. Math. Anal.*, **29** 1399–418, 1998.

[38] R. V. Sole, J. Valls, and J. Bascompte. Spiral waves, chaos and multiple attractors in lattice models of interacting populations. *Phys. Lett. A*, **166** 123 – 128, 1992.

[39] F. Veerman. Breathing pulses in singularly perturbed reaction diffusion systems. *Nonlinearity*, **28** 2211 – 2246, 2015.

[40] F. Verhulst. *Nonlinear Differential Equations and Dynamical Systems* Springer-Verlag Universitext, New York, 2006.

[41] J. Viventi, D. H. Kim, L. Vigeland *et al.* Flexible, foldable, actively multiplexed, high-density electrode array for mapping brain activity in vivo. *Nature Neuroscience*, **14** 1599–1607, 2011.

[42] A. T. Winfree. Rotating solutions to reaction-diffusion equations in simply-connected media. in *Mathematical aspects of chemical and biochemical problems and quantum chemistry (Proc. SIAM-AMS Sympos. Appl. Math., New York, 1974)*, 13–31. SIAM-AMS Proceedings, Vol. VIII, Amer. Math. Soc., Providence, R.I., 1974.

[43] A. T. Winfree. *The geometry of biological time.* Biomathematics **8**, Springer-Verlag, New York, 1980.

[44] C. Wulff, J. S. W. Lamb and I. Melbourne. Bifurcation from relative periodic solutions. *Ergodic Theory and Dynamical Systems*, **21** 605–635, 2001.

[45] J. Xu, R. Singh, N. Garnier, S. Sinha, and A. Pumir. The effect of quenched disorder on dynamical transitions in systems of coupled cells. *New Journal of Physics*, **15** 093046, 2013.

[46] Y.A. Yermakova and A.M. Pertsov. Interaction of Rotating Spiral Waves with a Boundary. *Biophys.*, **31** 932 – 940, 1986.

[47] V.S. Zykov and S.C. Müller. Spiral Waves on Circular and Spherical Domains of Excitable Medium. *Physica D*, **97** 322 – 332, 1996.